Non-hydrodynamic response in QCD-like plasma

Weiyao Ke[a] **and Yi Yin** ⓘ[b]

[a]*Key Laboratory of Quark and Lepton Physics (MOE) & Institute of Particle Physics,*
Central China Normal University,
Wuhan, Hubei, 430079, China

[b]*Quark Matter Research Center, Institute of Modern Physics, Chinese Academy of Sciences,*
Lanzhou, Gansu, 073000, China

E-mail: weiyaoke@ccnu.edu.cn, yiyin@impcas.ac.cn

Abstract: Quark-gluon plasma's (QGP) properties at non-hydrodynamic and non-perturbative regimes remain largely unexplored. Here, we examine the response functions describing how a QGP-like plasma responds to initial energy-momentum disturbance in both static and Bjorken-expanding plasma at non-hydrodynamic gradient using the Boltzmann equation in the relaxation-time approximation (RTA). We show that the resulting response functions are remarkably similar in both static and expanding backgrounds at non-hydrodynamic gradients. While non-hydrodynamic response can not be described by the conventional first-order and second-order theories, its behavior is reasonably captured by the extended version of hydrodynamics proposed by us [1]. The potential sensitivity of the Euclidean correlator to non-hydrodynamic response is also illustrated.

Contents

1 Introduction

When an in-homogeneous and time-dependent disturbance is created on the quark-gluon plasma (QGP), its response reveals the rich structure of the medium. The hydrodynamic theory should describe the medium's response in long wavelength and low-frequency limits. On the other hand, one could apply the perturbative QCD method to study QGP's behavior at an asymptotic large gradient. Apparently, exploring the intermediate regime between those two asymptotic limits is crucial to understanding how the properties of QCD matter evolve as scale changes. Yet, our knowledge about this non-hydrodynamic and possibly non-perturbative regime is very limited as illustrated in figure 1. See refs. [2–9] on examples of studying non-hydrodynamic properties of QGP.

Figure 1. A cartoon illustrating our current understanding of Quark-Gluon Plasma (QGP) as a function of the characteristic momentum scale (k). When k is small, QGP behaves like a near-perfect liquid. As k increases to the asymptotic free regime, QGP can be viewed as a parton gas. The properties of QGP at the intermediate scale are less known, but they can be explored by studying jet-medium interaction observables in heavy-ion collisions and by conducting the lattice QCD calculation of the Euclidean correlators, see further discussion in the text.

By comparing the behavior of conventional hydrodynamic theories extrapolated outside the hydrodynamic regime with QGP-like models, we may monitor how some hydrodynamic behavior disappears, and possible new features emerge as characteristic gradients gradually increase. Doing so can bring insight into the nature of the transition from QGP liquid to weakly-coupled parton gas. In this work, we will compare the non-hydrodynamic energy-momentum response obtained from the first-order and some variants of second-order hydrodynamics with that from a particular microscopic theory, which we consider the kinetic theory under relaxation time approximation (RTA). Despite its simplicity, the RTA kinetic theory captures a transition from the hydrodynamic regime to a regime whose response is dominated by quasi-particle excitations and has been widely used as a model for a QCD-like system. The study of the retarded correlator, which describes the medium's response induced by the metric perturbation using the Boltzmann equation, can be found in refs. [8, 10, 11]. Our focus is on the response function that describes the induced energy-momentum due to the initial energy-momentum disturbance.

Another motivation of our work is to further investigate and elaborate on the notion of the extended hydrodynamic regime (EHR) proposed by us in ref. [1], This scenario corresponds to the situation that a high-frequency sound exists that governs the medium's response outside the hydrodynamic regime on the one hand, and its dispersion is not described by naively extending conventional hydrodynamic theories outside the hydrodynamic scale on the other hand. In ref. [1], we demonstrate the presence of this scenario for strongly coupled $\mathcal{N} = 4$ super-symmetric Yang-Mills (SYM) theory and RTA kinetic theory. We also show that the sound dispersion can be captured by a "deformed" version of MIS, namely MIS*, with a suitable choice of model parameters. In this work, we show detailed analysis indicating that the same MIS* equations can describe not only dispersion relation but also response function outside the hydrodynamic regime.

Phenomenologically, the observables sensitive to the jet-medium interaction can help extract the medium's properties at a non-hydrodynamic scale. An energetic parton may be viewed as a point-like source that deposits energy and momentum density to the medium it transverses to. It would generate perturbation for a vast range of gradients, including those outside the hydrodynamic regime. Recently, evidence has been suggesting that properly incorporating the medium's response to those disturbances is essential in describing data (e.g., see refs. [12–16]). To date, many studies are using linearized first-order and second-order

hydrodynamics (or its variant) to account for the medium's response (see, for example, refs. [17–19]). We have analyzed the energy-momentum response for a Bjorken-expanding background. This allows us to compare the response functions for the static and expanding background and discuss the importance of non-hydrodynamic response in the context of jet-medium interaction.

Theoretically, one may extract the medium's properties from the Euclidean correlator, which can be studied from the first-principle lattice QCD calculations. While the Euclidean correlators are notoriously insensitive to the infrared structure of the real-time response (see ref. [20] for a review), it may be suitable for extracting response at a gradient of the order πT. We present perhaps the first illustrative analysis that suggests the sensitivity of the Euclidean correlator to the non-hydrodynamic response. Assuming the EHR scenario, we also explore the lattice's potential to extract the medium's properties in EHR.

This paper is organized as follows. In section 2.1, we derive a general relation between the response function describing the response induced by initial disturbance and the retarded correlator describing the medium's reaction to the metric perturbation, see eq. (2.10) (or eq. (2.11)). While it directly follows from the standard linear response theory, it seems new in the literature. We then compute the energy-momentum response function in a static background from RTA kinetic theory and hydrodynamic theories in sections 2.2 and 2.3 respectively. In section 3.1, we analyze the excitations that dominate the response for the RTA kinetic theory. In doing so, we review the concept of EHR and discuss its generality. Then we review the construction of MIS* in section 3.2. Section 3.3 compares kinetic response and that from different hydrodynamic theories. In section 4, we set up the formalism to calculate similar response functions in a Bjorken expanding background and present results in section 5. The sensitivity of the Euclidean correlator to non-hydrodynamic response is discussed and illustrated in section 6. Finally, we summarize in section 7.

Throughout this paper, we use the most plus metric $\eta^{\mu\nu} = (-1, 1, 1, 1)$.

2 Response in a static background

2.1 Response function and retarded correlator

We want to investigate the behavior of a thermal medium when it is in equilibrium and then undergoes an infinitesimally small perturbation. For definiteness, we look at a set of observables such as energy, and charge densities and collectively denoted the corresponding operator by $\hat{O}^I$ where I, J are the labels. In response to the perturbation, the expectation value $O = \langle \hat{O} \rangle$ will deviate from its equilibrium value $\langle \hat{O} \rangle_{\text{eq}}$, i.e. $\delta O = O - \langle \hat{O} \rangle_{\text{eq}} \neq 0$.

The present work primarily considers the response induced by the out-of-equilibrium deviation $\delta O_{\text{in}}^I(\boldsymbol{x}) \equiv \delta O^I(t = 0, \boldsymbol{x})$ at some initial time, say $t = 0$. To describe such a response, we define response function (R.F.) $\mathcal{G}$ as

$$\delta O^I(t, \boldsymbol{x}) = \int_{\boldsymbol{x}'} \mathcal{G}^I_J(t, \boldsymbol{x} - \boldsymbol{x}') \, \delta O_{\text{in}}^J(\boldsymbol{x}') \tag{2.1}$$

where $\int_{\boldsymbol{x}} \equiv \int d^3\boldsymbol{x}$ and the summation over the dummy index is understood. We shall assume that $\mathcal{G}$ satisfies the following initial condition:

$$\mathcal{G}^I_J(t = 0, \boldsymbol{x}) = \delta^I_J \, \delta^3(\boldsymbol{x}), \tag{2.2}$$

– 3 –

meaning we have assumed that when $I \neq J$, a non-zero δO_I will not cause a non-zero δO_J at the beginning. The discussion below can be easily generalized when this assumption is relaxed.

In parallel, the retarded correlator

$$G_R^{IJ}(t, t'; \boldsymbol{x}, \boldsymbol{x}') \equiv -i \Big\langle \left[\hat{O}^I(t, \boldsymbol{x}), \hat{O}^J(t', \boldsymbol{x}') \right] \Big\rangle \theta(t - t') \tag{2.3}$$

has been widely considered in literature. This correlator describes the response induced by the source $\psi_I(t, \boldsymbol{x})$ that is conjugate to $\hat{O}^I$ asuming that the perturbed Hamiltonian takes the form $\Delta \hat{H}(t) = -\int_{\boldsymbol{x}} \hat{O}^J(t, \boldsymbol{x}) \psi_J(t, \boldsymbol{x})$.

We can establish the relation between R.F. and the retarded correlator. The key observation is that $\mathcal{G}$ is entirely determined by the medium's properties and hence does not depend on how the initial deviation $\delta O_{\rm in}$ is created. We may generate $\delta O_{\rm in}^J$ by turning on the source ψ_J at $t = -\infty$ and switch it off at $t = 0$, i.e.,

$$\psi_J(t, \boldsymbol{x}) = \theta(-t) \, e^{-\epsilon t} \psi_{J,\rm in}(\boldsymbol{x}) \,, \tag{2.4}$$

where an infinitesimal value ϵ is introduced to ensure that the source vanishes at $t = -\infty$. Using the linear response theory (e.g., ref [21]), we then have, after taking spatial Fourier transform (assuming the translational invariance in space and time), that

$$\delta O^I(t, \boldsymbol{k}) = \int_{-\infty}^{\infty} dt' \, G_R^{IJ}(t - t', \boldsymbol{k}) \, \psi_J(t', \boldsymbol{k}) \,. \tag{2.5}$$

Particularly, evaluating eq. (2.5) at $t = 0$ with ψ_J specified by eq. (2.4) yields

$$\delta O_{\rm in}^I(\boldsymbol{k}) = \left(\int_{-\infty}^{0} dt' \, G_R^{IJ}(-t', \boldsymbol{k}) e^{\epsilon t'} \right) \psi_{J,\rm in}(\boldsymbol{k}) = \chi^{IJ}(\boldsymbol{k}) \, \psi_{J,\rm in}(\boldsymbol{k}) \,. \tag{2.6}$$

In other words, the induced $\delta O_{\rm in}^I$ resulting from turning on a time-independent source $\psi_{J,\rm in}$ from $t = -\infty$ to $t = 0$ is determined by the static susceptibility.

$$\chi^{IJ}(\boldsymbol{k}) = \int_0^{\infty} dt \, G_R^{IJ}(t, \boldsymbol{k}) = G_R^{IJ}(\omega = 0, \boldsymbol{k}) \,. \tag{2.7}$$

Now, we take the time derivative of eq. (2.5) w.r.t. time t. After using $\partial_t G_R(t - t') = -\partial_{t'} G_R(t - t')$ and performing the integration over t' by parts, we obtain (see also eq. 2.7 of ref. [21])

$$\partial_t \delta O^I(t, \boldsymbol{k}) = -G_R^{IJ}(t, \boldsymbol{k}) \psi_{J,\rm in}(\boldsymbol{k}) \,. \tag{2.8}$$

Assuming χ^{IJ} is invertible, we can rewrite (2.8) as

$$\partial_t \delta O^I(t, \boldsymbol{k}) = -G_R^{IJ'}(t, \boldsymbol{k}) \, (\chi^{-1}(\boldsymbol{k}))_{J'J} \delta O_0^J(\boldsymbol{k}) \,. \tag{2.9}$$

If we take the derivative of eq. (2.1) and compare it with eq. (2.9), we find the relation between the response function and retarded correlator that we are after:

$$\partial_t \mathcal{G}_J^I(t, \boldsymbol{k}) = -G_R^{IJ'}(t, \boldsymbol{k}) \, (\chi_R^{-1}(\boldsymbol{k}))_{J'J} \,. \tag{2.10}$$

Further performing the temporal Fourier transformation, we have

$$i\omega \mathcal{G}_J^I(\omega, \boldsymbol{k}) + \delta_J^I = G_R^{IJ'}(\omega, \boldsymbol{k})\,(\chi^{-1}(\boldsymbol{k}))_{J'J} \tag{2.11}$$

where we have used the property of "one-sided" Fourier transform

$$\int_0^\infty dt\, e^{i\omega t}\, \partial_t\, g(t) = -i\omega g(\omega, \boldsymbol{k}) - g_{\text{in}}\,. \tag{2.12}$$

for any function $g(t)$ satisfying $g(t = 0) = g_{\text{in}}$ and the initial condition for $\mathcal{G}$ (2.2) in the spatial Fourier space:

$$\mathcal{G}_J^I(t = 0, \boldsymbol{k}) = \delta_J^I\,. \tag{2.13}$$

Eqs. (2.10) and (2.11) are the main results of this section. They make it clear that one can determine the R.F. from the knowledge of the retarded correlator. In other words, how the medium reacts to the external source also tells us how it would respond to the initial perturbation. Moreover, the relation (2.11) reveals that the analytical structure of R.F. is the same as that of the retarded correlator. For instance, the pole of the correlator in the complex frequency plane should be the pole of R.F. at exactly the same location.

In the upcoming sections, we will discuss R.F. of the energy-momentum tensor (EMT):

$$\delta T^{\mu\nu}(t, \boldsymbol{k}) = \mathcal{G}^{\mu\nu}{}_{\alpha\beta}(t, \boldsymbol{k})\, \delta T_{\text{in}}^{\alpha\beta}(\boldsymbol{k})\,. \tag{2.14}$$

Our focus will be on a charge-neutral and conformal fluid. In this situation, there are only three independent components in $\mathcal{G}^{\mu\nu}{}_{\alpha\beta}$. Among them, one is associated with the behavior of shear stress. We will concentrate on the remaining two, which we choose to be[1]

$$\mathcal{G}_L(t, k) \equiv \mathcal{G}^{00}{}_{00}(t, k) \qquad \mathcal{G}_T(t, k) \equiv \mathcal{G}^{0x}{}_{0x}(t, k) \tag{2.15}$$

where without losing generality, we take the Fourier momentum $\boldsymbol{k}$ along z-direction.

2.2 Kinetic theory

The response function has to be computed from some microscopic theories to which we take the kinetic equation under relaxation time approximation (RTA)

$$p^\mu \partial_\mu f - \Gamma_{\alpha\sigma}^\lambda p^\alpha p^\sigma \frac{\partial f}{\partial p^\lambda} = -\frac{u \cdot p}{\tau_R}\,(f - f_{\text{eq}})\,. \tag{2.16}$$

Here, $f(t, \boldsymbol{x}, \boldsymbol{p})$ is the distribution of relativistic particles and $\Gamma_{\alpha\beta}^\lambda$ is the metric connection. The relaxation time τ_R sets the timescale at which f approaches the local equilibrium

$$f_{\text{eq}} \equiv e^{\beta p^\mu u_\mu}\,. \tag{2.17}$$

---

[1]It is well-known that by implementing Ward identity and rotational symmetry, the retarded correlator has only three independent components for a conformal system at finite temperature [22]. Among them is one representative component of shear stress correlator, while the other two can be identified as $G_R^{00,00} \sim \langle \delta T^{00} \delta T^{00} \rangle$ and $G_R^{0x,0x} \sim \langle \delta T^{0x} \delta T^{0x} \rangle$. The components of R.F. can be related to those of retarded correlator from the relation (2.11).

The local fluid velocity, u^μ together with energy density ϵ, are determined by the matching condition

$$T^{\mu\nu} = \int_{\boldsymbol{p}} \frac{1}{p} p^\mu p^\nu f , \qquad T^{\mu\nu} u_\nu = \epsilon u^\mu . \tag{2.18}$$

where $\int_{\boldsymbol{p}} \equiv \int d^3\boldsymbol{p}/(2\pi)^3$, and for ultra-relativistic particle, we have $p = |\boldsymbol{p}|$. With ϵ given, the effective temperature $T = 1/\beta$ in eq. (2.17) is determined by assuming the equation of state for the relativistic Boltzmann gas, i.e., $\epsilon(T) = N_0(3T^4)/\pi^2$ where N_0 counts the quantum state and species of particles under consideration, although the results shown in the present paper do not depend on the value of N_0. For the system to be conformal system, we require τ_R scales with ϵ

$$\tau_R \sim (\epsilon)^{-1/4} . \tag{2.19}$$

We shall study R.F. (2.15) describing the induced energy density and fluid velocity around the equilibrium background

$$\epsilon = \epsilon_0 + \delta\epsilon , \qquad u^\mu = (1, \boldsymbol{0}) + (0, \delta\boldsymbol{u}) , \tag{2.20}$$

where we use subscript 0 to denote the background value of thermodynamic and fluid variables such as ϵ, u^μ. Using

$$\delta f_{\text{eq}} = e^{-\beta_0 p^0} \left(-p_0 \delta\beta + \beta_0 \, \boldsymbol{p} \cdot \delta\boldsymbol{u} \right) \tag{2.21}$$

we have

$$\left(\partial_t + \boldsymbol{v} \cdot \boldsymbol{\partial} + \tau_R^{-1} \right) \delta f = \beta p_0 f_0 \, \tau_R^{-1} \left[-\frac{\delta\beta}{\beta} + \delta\boldsymbol{u} \cdot \boldsymbol{v} \right] . \tag{2.22}$$

where we have introduced the short-handed notation $f_0 \equiv e^{-\beta_0 p^0}$ for the background equilibrium distribution and $\boldsymbol{v} = \hat{p}$ is the single particle velocity. We shall solve eq. (2.22) under the initial condition that the distribution is in local equilibrium:

$$\delta f_I = \delta \, e^{\beta(p \cdot u)} = \beta_0 p^0 f_0 \left(\frac{-\delta\beta_I}{\beta_0} + \delta\boldsymbol{u}_I \cdot \boldsymbol{v} \right) , \tag{2.23}$$

where $\delta\boldsymbol{u}_I, \delta\beta_I$ denotes the value of $\delta\boldsymbol{u}, \delta\beta$ at $t = 0$. The solution to eq. (2.22) in Fourier space then reads

$$\delta f(\bar{\omega}, \bar{k}; \boldsymbol{v}) = \frac{i \, \beta_0 p_0 f_0 \tau_R^{-1}}{(\omega - \boldsymbol{v} \cdot \bar{\boldsymbol{k}} + i\tau_R^{-1})} \left[\left(-\frac{\delta\beta(\bar{\omega}, \bar{\boldsymbol{k}})}{\beta_0} + \delta\boldsymbol{u}(\bar{\omega}, \bar{\boldsymbol{k}}) \cdot \boldsymbol{v} \right) + \frac{\delta f_I(\bar{\boldsymbol{k}}; \boldsymbol{v})}{\beta_0 p_0 f_0 \tau_R^{-1}} \right] . \tag{2.24}$$

where $\bar{\omega} = \omega\tau_R$ and $\bar{k} = k\tau_R$. Plug in the Fourier transform of the initial condition, and further use the relation $\beta^2 \delta\epsilon = -c_V \delta\beta$ with $c_V = \partial\epsilon/\partial T$ being the specific heat, we arrive at

$$\delta f(\bar{\omega}, \bar{k}) = \frac{i \, \beta_0 p_0 f_0}{(\bar{\omega} - \boldsymbol{v} \cdot \bar{\boldsymbol{k}} + i)} \left[\frac{\beta_0 \delta\epsilon(\bar{\omega}, \bar{\boldsymbol{k}})}{c_V} + \delta\boldsymbol{u}(\bar{\omega}, \bar{\boldsymbol{k}}) \cdot \boldsymbol{v} + \left(\frac{\beta_0 \delta\epsilon_I(\bar{\boldsymbol{k}})}{c_V} + \delta\boldsymbol{u}_I(\bar{\boldsymbol{k}}) \cdot \boldsymbol{v} \right) \tau_R \right] . \tag{2.25}$$

Note that the mass dimension of $\delta\boldsymbol{u}(\bar{\omega}, \bar{k})$ is -4 while that of $\delta\boldsymbol{u}_I(\bar{k})$ is -3.

We are now ready to determine the R.F.. For the response in the longitudinal channel, we consider non-zero $\delta\epsilon, \delta u^z$ where, as we mentioned earlier, we shall take $\boldsymbol{k}$ along the z-direction. We are interested in computing energy-energy response function $\mathcal{G}_L$ (2.15) so we use the initial condition $(\delta\epsilon, \delta u^z) = (\delta\epsilon_{\text{in}}, 0)$ at $t = 0$ in accordance with eq. (2.2)) Substituting eq. (2.24) into the linearized version of eq. (2.18),

$$\delta T^{\mu\nu} = \int_{\boldsymbol{p}} \frac{p^\mu p^\nu}{p}\, \delta f \,, \tag{2.26}$$

and use the relation

$$\delta\epsilon = \delta T^{00}, \qquad \delta T^{0i} = w_0 \delta u^i \tag{2.27}$$

where $w = \epsilon + P$ is the enthalpy density, we find

$$\delta\epsilon(\omega, \boldsymbol{k}) = C_0(\omega, \boldsymbol{k})(\delta\epsilon(\omega, \boldsymbol{k}) + \delta\epsilon_{\text{in}}(\boldsymbol{k})\tau_R) + \frac{1}{c_s^2}\, C_1(\omega, \boldsymbol{k})\, \delta T^{0z}(\omega, \boldsymbol{k}) \,, \tag{2.28a}$$

$$\delta T^{0z}(\omega, \boldsymbol{k}) = C_1(\omega, \boldsymbol{k})(\delta\epsilon(\omega, \boldsymbol{k}) + \epsilon_{\text{in}}(\boldsymbol{k})\tau_R) + \frac{1}{c_s^2}\, C_2(\omega, \boldsymbol{k})\, \delta T^{0z}(\omega, \boldsymbol{k}) \,. \tag{2.28b}$$

Here, we have used the expression for c_V

$$c_V = \int_{\boldsymbol{p}} p \frac{\partial f_0}{\partial T} = \beta^2 \int \frac{dp}{2\pi^2}\, p^2 f_0 \tag{2.29}$$

which leads to the following useful expression

$$\int \frac{dp}{2\pi^2}\, \beta_0 p^2 f_0 (-\frac{\delta\beta}{\beta_0})\,(\dots) = \beta_0^{-2}\, c_V(-\delta\beta) \int \frac{d\Omega}{4\pi}\,(\dots) = \delta\epsilon \int \frac{d\Omega}{4\pi}\,(\dots) \tag{2.30a}$$

$$\int \frac{dp}{2\pi^2}\, \beta_0 p^2 f_0\, \delta u^i\,(\dots) = \frac{\delta T^{0i}}{w_0} \beta_0^{-2}\, c_V \int \frac{d\Omega}{4\pi}\,(\dots) = \frac{\delta T^{0i}}{c_s^2} \int \frac{d\Omega}{4\pi}\,(\dots) \,, \tag{2.30b}$$

Here, $d\Omega = d\phi\, d\cos\theta$ denotes the integration over the solid angle in the phase space, and $(\dots)$ refer to any functions which only depend on $\hat{p} = (\sin\theta\cos\phi, \sin\theta\cos\phi, \cos\theta)$. The sound velocity is denoted by c_s^2 and obeys the relation $c_V T/w = 1/c_s^2$. In eq. (2.28), functions C_n are defined by

$$C_n \equiv \frac{1}{2} \int_{-1}^{1} d\cos\theta \frac{i\cos^n\theta}{\bar{\omega} - \bar{k}\cos\theta + i} \,. \tag{2.31}$$

Solving eq. (2.28) for $\delta\epsilon, \delta\boldsymbol{u}$ and using $c_s^2 = 1/3$ yields $\delta\epsilon$ induced by the initial energy disturbance

$$\delta\epsilon = \frac{-\left(-3C_1^2 + 3C_0 C_2 - C_0\right)\epsilon_{\text{in}}(\boldsymbol{k})\tau_R}{-3C_1^2 + 3C_0 C_2 - C_0 - 3C_2 + 1} \,, \tag{2.32}$$

from which we read the response function

$$\mathcal{G}_L(\omega, k) = \frac{-\left[6\bar{k} + \left(3(i + \bar{\omega}) + i\bar{k}^2\right) L(\bar{\omega}, \bar{k})\right]\tau_R}{2\bar{k}(\bar{k}^2 + 3i\bar{\omega}) + i\left(\bar{k}^2 + 3\bar{\omega}(i + \bar{\omega})\right) L(\bar{\omega}, \bar{k})} \,. \tag{2.33}$$

Here, for convenience, we have defined

$$L(\omega, k) = \ln\left(\frac{\bar{\omega} - \bar{k} + i}{\bar{\omega} + \bar{k} + i}\right). \tag{2.34}$$

and used the relation among C_ns.

$$C_0 = \frac{-i}{2\bar{k}} L(\bar{\omega}, \bar{k}), \qquad C_1 = \frac{-i}{\bar{k}}\left(1 - (1 - i\bar{\omega})C_0\right). \tag{2.35a}$$

$$C_2 = \frac{1}{\bar{k}}\left(i + \bar{\omega}\right)C_1 = \frac{(1 - i\bar{\omega})}{\bar{k}^2}\left(1 - (1 - i\bar{\omega})C_0\right). \tag{2.35b}$$

Similarly, we find that in the transverse channel

$$\mathcal{G}_T(\omega, k) = \frac{3i\left[2\bar{k}(\bar{\omega} + i) - \left(\bar{k}^2 + (1 - i\bar{\omega})^2\right)L(\bar{\omega}, \bar{k})\right]\tau_R}{2\bar{k}(3 + 2\bar{k}^2 - 3i\bar{\omega}) + 3i\left(\bar{k}^2 + (1 - i\bar{\omega})^2\right)L(\bar{\omega}, \bar{k})}. \tag{2.36}$$

The expression for the RTA retarded correlators has been obtained in ref. [23], see also ref. [8]. We copy the relevant expression in terms of $C_{0,1,2}$ below (up to a contact term) in our notation:

$$G_R^{00,00}(\omega, k) = 3w_0 \frac{i\bar{k}C_1}{-3C_1^2 + 3C_0C_2 - C_0 - 3C_2 + 1}, \tag{2.37}$$

$$G_R^{0x,0x}(\omega, k) = -3w_0 \frac{i\bar{\omega}(C_0 - C_2)}{2 - 3(C_0 - C_2)}. \tag{2.38}$$

Using the expressions (2.33) and (2.36), one can verify the relation (2.11) between the response function and the retarded correlator.

2.3 Hydrodynamic response function

The primary goal of this paper is to investigate the response function's behavior beyond the hydrodynamic regime. To benchmark hydrodynamic behavior, we now calculate $\mathcal{G}_L$ and $\mathcal{G}_T$ within hydrodynamics and/or its cousin theory, Muller, Israel and Stewart (MIS) theory. In the following section, we will compare these results with the RTA response.

We begin with the decomposition of EMT

$$T^{\mu\nu} = \epsilon u^\mu u^\nu + P\Delta^{\mu\nu} + \pi^{\mu\nu} \tag{2.39}$$

where p denotes the pressure, and the projector is given by

$$\Delta^{\mu\nu} = \eta^{\mu\nu} + u^\mu u^\nu, \tag{2.40}$$

and $\pi^{\mu\nu}$ arise from the gradient correction to $T^{\mu\nu}$. For a conformal fluid, $P = \epsilon/3$ and $\pi^{\mu\nu}$ is traceless. One may expand $\pi^{\mu\nu}$ in gradient in the long time and wavelength limit. To the first-order gradient, $\pi^{\mu\nu}$ takes the form

$$\pi_{(1)}^{\mu\nu} = -2\eta\,\sigma^{\mu\nu} \tag{2.41}$$

where η is the shear viscosity, and the shear stress is given by

$$\sigma^{\mu\nu} = \nabla^{\langle\mu} u^{\nu\rangle} \,. \tag{2.42}$$

Here ∇^μ denotes the covariant derivative. Angular brackets around a pair of Lorentz indices, $^{\langle\mu\nu\rangle}$, mean that the indices are to be symmetrized, space-projected, and trace-subtracted, i.e.:

$$A^{\langle\mu\nu\rangle} = \frac{1}{2}\Delta^{\mu\alpha}\Delta^{\mu\beta}\left(A_{\alpha\beta} + A_{\beta\alpha}\right) - \frac{1}{3}\Delta^{\mu\nu}\Delta^{\alpha\beta}A_{\alpha\beta} \,. \tag{2.43}$$

As usual, we refer to the conservation equation

$$\nabla_\mu T^{\mu\nu} = 0 \tag{2.44}$$

supplemented by the relation $\pi^{\mu\nu} = \pi^{\mu\nu}_{(1)}$ (2.41) as the first-order hydrodynamics for a charge-neutral system. One may include contributions from higher-order gradient terms [24–26]. Various versions of higher-order theories have shared a feature that $\pi^{\mu\nu}$ is promoted as an independent dynamical degree of freedom. For the theory developed by Muller, Israel and Stewart (MIS), $\pi^{\mu\nu}$ obeys a simple relaxation equation:

$$D\pi^{\mu\nu} = -\frac{1}{\tau_\pi}\left(\pi^{\mu\nu} - \pi^{\mu\nu}_{(1)}\right) \,, \tag{2.45}$$

where $D \equiv u \cdot \nabla$ is the time-derivative in the fluid rest-frame and τ_π gives the relaxation time scale under which $\pi^{\mu\nu}$ approaches $\pi^{\mu\nu}_{(1)}$.

We first consider the response function in the longitudinal channel obtained from linearizing hydrodynamic theories. As we did earlier, we take k along z-direction. Therefore the relevant dynamical fields are $\delta\epsilon, \delta u^z, \pi^{zz}$ where shall count π^{ij} as $\mathcal{O}(\delta)$. To compute $\mathcal{G}_L$ (2.15), it is sufficient to consider the initial condition $\left.(\delta\epsilon, \delta u^z, \pi^{zz})\right|_{t=0} = (\delta\epsilon_{\mathrm{in}}, 0, 0)$.

By linearizing conservation equation (2.44) and evolution equation for $\pi^{\mu\nu}$ (2.45) and the performing the Fourier transform, we have

$$-i\omega\frac{\delta\epsilon}{w_0} = -ik\delta u^z + \frac{\delta\epsilon_{\mathrm{in}}}{w_0} \,, \tag{2.46a}$$

$$-i\omega\,\delta u^z = -ik\left(c_s^2\frac{\delta\epsilon}{w_0} + \frac{\pi^{zz}}{w_0}\right) \,, \tag{2.46b}$$

$$-i\omega\frac{\pi^{zz}}{w_0} = -\frac{1}{\tau_R}\left(\frac{\pi^{zz}}{w_0} + ik\frac{4}{3}\nu_0\,\delta u_z\right) \,, \tag{2.46c}$$

where specific viscosity is given by $\nu = \eta/w$. To obtain eq. (2.46a), we have used eq. (2.12). Now, we solve eq. (2.46c) to find

$$\frac{\pi^{zz}}{w_0} = -\nu(\omega)\,ik\delta u^z \,, \tag{2.47}$$

where we have defined frequency-dependent longitudinal momentum diffusive coefficient

$$\nu(\omega) = \frac{4}{3}\frac{\nu_0}{1 - i\omega\tau_\pi} \,, \tag{2.48}$$

Substituting eq. (2.47) into eq. (2.46b) and using eq. (2.46a) yields

$$\delta\epsilon(\omega, k) = \frac{1}{R(\omega, k)} \left(i\omega - \nu(\omega)k^2 \right) \delta\epsilon_{\text{in}}(\omega, k) \,, \tag{2.49}$$

where

$$R(\omega, k) = \omega^2 - c_s^2 k^2 + i\nu(\omega)\omega k^2 \,. \tag{2.50}$$

We then arrived at the expression for the longitudinal response function

$$\mathcal{G}_L(\omega, k) = \frac{i\omega - \nu(\omega)k^2}{R(\omega, k)} \,. \tag{2.51}$$

In parallel, we find

$$\mathcal{G}_T(\omega, k) = \frac{i}{\omega + i\nu_T(\omega)\, k^2} \,, \tag{2.52}$$

where frequency-dependent transverse momentum diffusive coefficient reads (cf. eq (2.48))

$$\nu_T(\omega) = \frac{\nu_0}{1 - i\omega\tau_\pi} \,. \tag{2.53}$$

It is easy to verify that the above hydrodynamic expressions can be matched to the small ω, k behavior of RTA response function (2.33), (2.36) with

$$c_s^2 = \frac{1}{3} \,, \qquad \nu_0 = \frac{1}{5}\tau_R \qquad \tau_\pi = \tau_R \tag{2.54}$$

Before closing, we recall the related EMT correlators in the hydrodynamics regime (see e.g., refs. [10, 11]) is given by (up to the ω, k-independent contact terms)

$$G_R^{00,00}(\omega, k) = \frac{w_0 k^2}{R(\omega, k)} \,, \qquad G_R^{0x,0x}(\omega, k) = \frac{-iw_0\, \nu_T(\omega)k^2}{\omega + i\nu_T(\omega)k^2} \tag{2.55}$$

It is then straightforward to confirm the relation between the response function and the retarded correlator (2.11).

3 Extended hydrodynamic regime

3.1 Excitations

The behavior of the R.F. is determined by the properties of the medium's excitations that can be recognized by studying its analytic structure (pole, branch-cut) in the complex ω-plane. In physical terms, poles indicate the collective modes and the branch-cuts are typically associated with quasi-particle excitations. In the time domain,

$$\mathcal{G}(\Delta t, k) = \int_{-\infty}^{\infty} \frac{d\omega}{2\pi}\, \mathcal{G}(\omega, k)e^{-i\omega\Delta t} \tag{3.1}$$

we can close the contour of the integration over ω in the lower half-plane to explicitly show the contributions of the pole and branch cut,

$$\mathcal{G}(\Delta t, k) = -i\sum_n \mathcal{R}_n(k)e^{-i\omega_n\Delta t} + \sum_m \oint_{\mathcal{C}_m} \frac{d\omega}{2\pi}\mathcal{G}(\omega, k)e^{-i\omega\Delta t} \,, \tag{3.2}$$

where all the poles and branch cuts are labeled by n and m, respectively. Here, $\mathcal{R}_n(k)$ is the residue of the $\mathcal{G}(\omega, k)$ at pole $\omega = \omega_n(k)$. $\mathcal{C}_m$ schematically denote the contour around the branch-cut m.

Specifically, the RTA response function has poles given by the zeros of the denominator in eqs. (2.33), (2.36):

$$2\bar{k}\left(\bar{k}^2 + 3i\bar{\omega}\right) + i\left(\bar{k}^2 + 3\bar{\omega}(i + \bar{\omega})L(\bar{\omega}, \bar{k})\right) = 0\,, \tag{3.3a}$$

$$2\bar{k}\left(3 + 2\bar{k} - 3i\bar{\omega}\right) + 3i\left(\bar{k}^2 + (1 - i\bar{\omega})^2\right)L(\bar{\omega}, \bar{k}) = 0\,, \tag{3.3b}$$

for the longitudinal and transverse channels, respectively. In the longitudinal channel (3.3a), the solutions present a pair of propagating modes (sound-like modes) $\omega_L(k) = \pm v(k)k - i\Gamma(k)$ where v is the phase velocity and Γ is the attenuation rate. In the transverse sector (3.3b), the solution is purely imaginary $\omega_T = -i\Gamma_T(k)$. In the regime where k is small, RTA collective modes are usual hydrodynamic sound and shear modes (see also figure 3 below). Nevertheless, as first noticed in ref. [23], collective modes in RTA continue to exist until $\bar{k} = \bar{k}_O$ with $\bar{k}_O = 4.52$ for the longitudinal channel and $\bar{k}_O = 3\pi/4 = 2.37$ for the transverse channel. We refer to those modes outside the hydrodynamic regime as high-frequency sound and shear modes for the clarity of presentation and for the reasons that will be revealed later in section 3.1.1.[2]

Besides the poles, $\mathcal{G}_{L,T}$ have a logarithmic branch cut stretching from $\bar{\omega} = -\bar{k} - i$ to $\bar{\omega} = \bar{k} - i$ (see the expression of L (2.34)). They represent quasi-particle excitations through the effect akin to Landau-damping; see section IIB of ref. [8] for an intuitive elaboration on their origin. For $\bar{k} > \bar{k}_O$, the response of the medium is determined solely by quasi-particle excitations. At the same time, hydrodynamic modes govern for $\bar{k} < k_H \tau_R$, with k_H denoting the boundary of the hydrodynamic regime. The question of interest, therefore, is, what is the relative importance of "high-frequency" sound and shear modes and quasi-particle excitations in the intermediate regime $k_H < \bar{k} < \bar{k}_O$?

In figure 2, which exhibits the RTA response function vs Δt for three values of $\bar{k}$ ($\bar{k} < \bar{k}_O$) in the longitudinal and transverse channel, we have shown the contribution from the poles and branch cuts separately. Remarkably, the collective modes have a prevalent impact on the behavior of response functions even at the non-hydrodynamic gradient, especially at sufficiently large t. To understand why this happens, we compared the damping rate of RTA collective modes with the relaxation rate of quasi-particle excitations shown in figure 3. We refer to the difference between the two, $\Delta\Gamma(k) = \tau_R^{-1} - \text{Im}(\omega(k))$, as the gap. If the gap is greater than zero, the contribution from quasi-particle excitations will be suppressed by $\exp(-\Delta\Gamma\Delta t)$, eventually making high-frequency hydrodynamic modes dominate the response.

---

[2]It is fun to note that the high-frequency sound mode may be viewed as analogous of Tiktaalik in the context of biological evolution. According to Wikipedia (https://en.wikipedia.org/wiki/Tiktaalik), "its fins have thin ray bones for paddling like most fish, but they also have sturdy interior bones that would have allowed Tiktaalik to prop itself up in shallow water and use its limbs for support as most four-legged animals do. Those fins and other mixed characteristics mark Tiktaalik as a crucial transition fossil, a link in evolution from swimming fish to four-legged vertebrates". Similarly, the high-frequency sound mode propagates as a sound mode but with a phase velocity closer to the velocity of parton than the ordinary sound. It might be the crucial link in the evolution of excitations in a QGP-like plasma from hydrodynamic modes to the weakly-coupled quasi-particles.
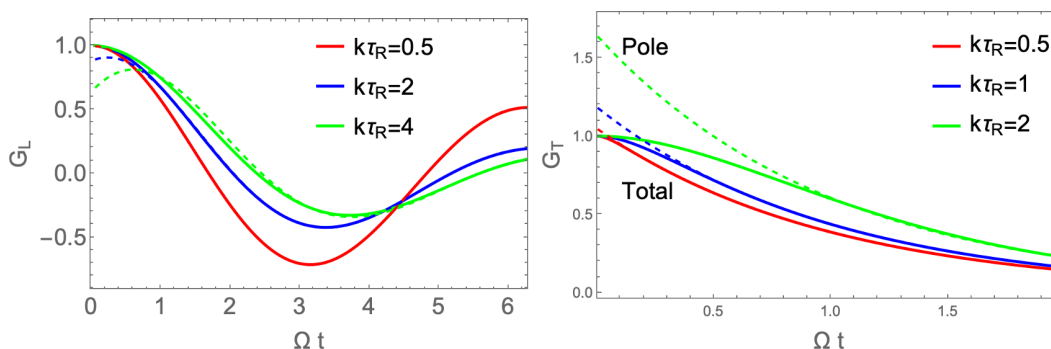
Figure 2. RTA response function in the time domain (solid curves) at three different values of $\bar{k} = k\tau_R$. They are compared with the contribution from the collective modes $\omega_L(k), \omega_T(k)$ (dashed curves), which are conventional sound and shear modes in hydrodynamic regime (see eq. (3.2) and the text). In the extended hydrodynamic regime for RTA kinetic theory where $\bar{k} \geq 1$, those modes are referred to as high-frequency sound and shear mode. (Left): the longitudinal channel where we have rescaled the time by $\Omega = |\mathrm{Re}\Omega_L(k)|$ (Right): the transverse channel where we have rescaled the time by $\Omega = |\mathrm{Im}\Omega_T(k)|$.
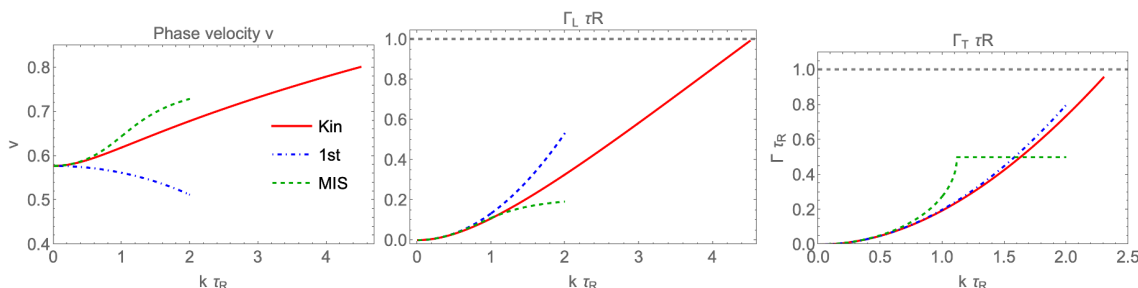
Figure 3. The dispersion of collective modes in RTA kinetic theory. In the longitudinal channel, the solution to eq. (3.3a) represents a propagating mode $\omega_L(k) = \pm v(k)\,k - i\Gamma(k)$. In the transverse channel, the solution to eq. (3.3b) is purely dissipative $\omega_T(k) = -i\Gamma_T(k)$. From left to right, the red curves in the figure correspond to phase velocity v, attenuation rate Γ, and Γ_T as a function of $\bar{k} = k\tau_R$. For comparison, the first-order hydrodynamics and MIS theory results are plotted in blue dashed and green dotted curves, respectively. For figures on the middle and left, the horizontal black dashed curves plot the damping rate of quasi-particle excitations, $1/\tau_R$.

The gap remains open unless the value of $\bar{k}$ is close to $\bar{k}_O$, as seen in figure 3, which explains the importance of high-frequency sound and shear modes outside the hydrodynamic regime.

It is crucial to mention that the dispersion of those high-frequency collective modes can not be described by extrapolating the results in the usual hydrodynamic theories to a larger gradient. To elucidate this, we compute the poles of the hydrodynamic response functions (2.51), (2.52) by solving

$$R(\omega, k) = \omega^2 - c_s^2 k^2 + i\nu(\omega)\omega k^2 = 0\,, \tag{3.4a}$$

in the longitudinal channel and

$$\omega + i\nu_T(\omega)\,k^2 = 0\,. \tag{3.4b}$$

in the transverse channel. Here $\nu(\omega)$ equals to ν_0 for the first-order theory and is given by (2.48) in MIS theory, and the relevant transport coefficients are listed in eq. (2.54). In figure 3, we confirm that first-order and MIS theory accurately describes the dispersion of the RTA collective modes in the hydrodynamic regime but generally fall short in capturing important qualitative features of the RTA modes as we move to a larger gradient, see also further discussion in section 3.3.

3.1.1 Extended hydrodynamic regime: generalities

More generally, one may introduce the notion of "Extended Hydrodynamic regime" (EHR), as discussed recently in ref. [1]. EHR has two defining properties: 1) high-frequency sound and/or shear modes exist that are gapped from other non-hydrodynamic excitations; 2) the dispersion relation of high-frequency sound and shear mode can not be described by conventional hydrodynamic theory. The RTA kinetic theory exemplifies the existence of EHR, as discussed in the preceding sections.

Importantly, EHR can appear in a wide range of microscopic theories.

First of all, the authors of refs. [27, 28] demonstrate remarkable agreement among the retarded correlator in the sound channel for kinetic theory with different collision kernels once time and gradient are rescaled by the effective relaxation time η/w. Those collision kernels include those obtained from RTA, scalar ϕ^4, SU(3) Yang-Mills theory and QCD effective kinetic theory with $N_f = 3$. This study indicates that EHR, observed using the simplified RTA collision kernel, applies to more sophisticated and realistic collision kernels derived from quantum field theory.

Furthermore, high-frequency sound mode is not uncommon in strongly coupled gauge theories that can be calculated using holography duality. For example, in the strongly coupled $\mathcal{N} = 4$ super-symmetric Yang-Mills theory in large N_c limit (SYM), which captures many features of QCD in strong coupling, the sound mode exists at any finite gradient and has a smaller than damping rate than other excitations (quasi-normal modes) [29, 30]. This similarity between kinetic theory and strongly coupled SYM theory is remarkable, given that the coupling strength is drastically different between the two.

Finally, various liquid metals can sustain sound modes extending from hydrodynamic regime to wavelengths comparable to inter-atomic distances, as reviewed in refs. [31, 32]. All the results discussed above indicate the generality of the EHR scenario.

3.2 The construction of MIS*

We review MIS* theory, which we proposed in ref. [1]. The purpose of constructing MIS* is to provide a simple model that can describe the response in EHR. Our approach is by "trial and error" strategy: we explore the simplest extension of MIS and evaluate its effectiveness. The resulting theory may be seen as a "deformation" of MIS theory that we decompose the non-equilibrium corrections to the EMT, $\pi^{\mu\nu}$ (2.39), into two parts:

$$\pi^{\mu\nu} = \pi_1^{\mu\nu} + \pi_2^{\mu\nu}, \tag{3.5}$$

And we require the dynamic equation for $\pi_{1,2}$ to have the same form as eq. (2.45) in MIS theory.:

$$D\pi_a^{\mu\nu} = -\frac{1}{\tau_a}\left(\pi_a^{\mu\nu} + 2\eta_a\,\sigma^{\mu\nu}\right), \qquad a = 1, 2, \tag{3.6}$$

where $\eta_{1,2}, \tau_{1,2}$ are model parameters. Without losing generality, we shall assume that $\tau_1 < \tau_2$, meaning π_2 relaxes faster than π_1. In the long time limit, $\pi^{\mu\nu}$ should approach to its value in the first-order hydrodynamics (2.41), yielding the following constraint

$$\sum_{a=1}^{2} \eta_a = \eta. \tag{3.7}$$

We shall examine if MIS* can be used to describe EHR response in RTA kinetic theory. Following a similar procedure as in section 2.3, we find $\mathcal{G}_L, \mathcal{G}_T$ from MIS* is of the same form as eqs. (2.51) and (2.52), respectively, with $\nu(\omega), \nu_T(\omega)$ given by

$$\nu(\omega) = \frac{4}{3}\sum_{a=1}^{2}\frac{\nu_a}{1 - i\omega\tau_a}, \qquad \nu_T(\omega) = \frac{3}{4}\nu(\omega). \tag{3.8}$$

where $\nu_a = \eta_a/w_0$. To further simplify the model, we consider the limit $\tau_2/\tau_1 \to 0$, allowing eq. (3.8) to be written as

$$\nu(\omega) = \frac{4\nu_0}{3}\left(\frac{1 - \delta}{1 - i\omega\tau_1} + \delta\right). \tag{3.9}$$

where two dimensionless ratios are defined for later convenience

$$\delta = \frac{\eta_2}{\eta}, \qquad \gamma = \frac{\tau_1}{\tau_\pi}. \tag{3.10}$$

This limit means that even at non-hydrodynamic timescales like $\omega \sim \tau_1^{-1}$, $\pi_2^{\mu\nu}$ has enough time to relax to $-2\eta_2\sigma^{\mu\nu}$ and contribute around $\propto \delta k^2$ to the damping rate of sound mode, which makes δ the parameter that controls the dissipative rate in EHR.[3] We note that while τ_π in MIS theory is fixed by matching to the second-order hydrodynamics, we only require MIS* to reproduce the first-order hydrodynamic results and not higher-order corrections in the small gradient limit. With this little compromise, we could adjust τ_1 or the ratio γ to describe modes in EHR, making it an excellent trade-off, as we shall see shortly.

3.3 Kinetic theory vs. hydrodynamic theories

In this section, we will explore how the RTA response function behaves in a static and homogeneous equilibrium background in the time domain. To do so, we will use equation (3.1) alongside eqs. (2.33) and (2.36). We will then compare these results with their counterpart in the Bjorken expanding background in section 5. Moreover, we will compare the RTA results with responses in "hydrodynamic theories", which include first-order MIS and MIS*

---

[3]Like MIS theory, MIS* is not causal for very large k in the $\tau_2 \to 0$ limit, but this is not a severe problem as long as we are working on the linear response regime. We can use a small but finite value of r to ensure causality if necessary.
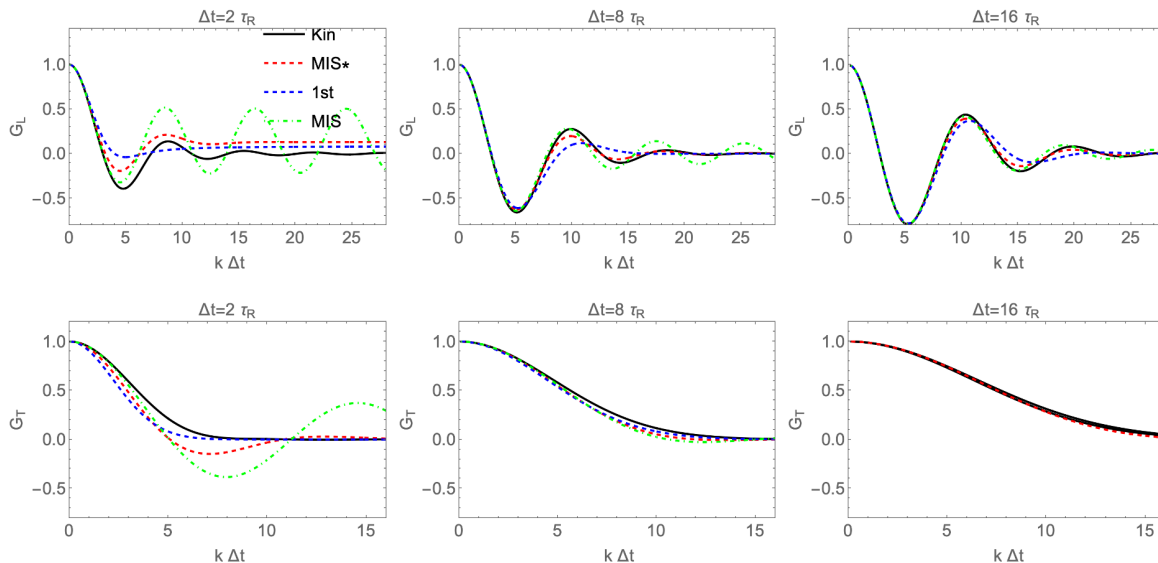
Figure 4. The RTA response function vs $k\Delta t$ for the longitudinal channel (the upper panel) and the transverse channel (the lower panel). For comparison, MIS* (obtained by choosing $(\delta, \gamma) = (0.15, 0.8)$), MIS, and the first-order hydrodynamic results are shown in red, blue, and green curves, respectively. For their analogs in the Bjorken expanding background, see figure 6.

theory. We put a quotation mark here to emphasize that some of those theories are to be extrapolated outside the hydrodynamic regime. The first-order and MIS theory results are obtained using parameters listed in eq. (2.54). For MIS*, we will use a suitable choice of (γ, δ), which could describe RTA sound dispersion; see figure 1 in ref. [1].

In figure 4, we show the longitudinal (the upper panel) and transverse (the lower panel) response function vs k for $\Delta t = 2\,\tau_R$ (left), $\Delta t = 8\,\tau_R$ (middle) and $\Delta t = 16\,\tau_R$ (right). They represent early-time, intermediate-time, and late-time responses, respectively. For kinetic theory, $\mathcal{G}_L$ exhibits the damped oscillation behavior while $\mathcal{G}_T$ is purely dissipative. As k increases, Hydrodynamic and RTA kinetic theory start to differentiate from each other. MIS theory, which includes higher-order gradient effects, only modestly improves the description when k is small. Outside the hydrodynamic regime, both first-order and MIS theory are inadequate to describe the RTA response (see also ref. [10]). The discrepancy can be primarily explained by the difference in the dispersion of collective modes among those theories. For instance, the phase velocity $v(k)$ of RTA sound mode rises from the conformal sound velocity $\sqrt{1/3} \approx 0.57$ up to 0.8 as k increases, and the sound attenuation rate also rises with k. In contrast, (extrapolated) first-order hydrodynamics does not give a supersonic phase velocity, and the sound damping rate grows faster than the RTA theory. Consequently, as shown in figure 4, first-order hydrodynamics is less oscillatory with a smaller amplitude than the RTA response function. As for the MIS theory, the phase velocity of the sound mode also increases, but its attenuation rate will be saturated instead of growing as k becomes larger. This explains the oscillating behavior in the MIS response function at large k where RTA sound mode has already been damped out.

Suppose we define "hydrodynamization" of response as the point where the response function closely matches the hydrodynamic prediction at a specific Δt.[4] In that case, we can see that in the shear channel, hydrodynamization occurs sooner than in the sound channel. There are at least two reasons why this may occur. The first reason is accidental: the shear dispersion happens to be quantitatively similar in the first-order and RTA theory for a wide range of values for k. The second one is more general. The damping rate of the shear mode is greater than that in the sound channel at given k. Therefore, the non-hydrodynamic gradient will be damped first in the former sector. It is worthwhile mentioning that in the transverse channel, equation (3.4b) has two roots at a fixed value of k. While both modes are imaginary for small k, they become a pair of propagating modes for k larger than a certain threshold. This is responsible for the spurious wave-like behavior observed in the MIS response function in the shear channel.

In figure 4, we illustrate the comparison between RTA and MIS* response function with a representative combination of model parameters $(\gamma, \delta) = (0.25, 0.8)$. Despite the model's simplicity, the agreement in the sound channel is rather remarkable. In the shear channel, the agreement is less impressive. Pursuing improvement in this channel is interesting, which we leave to future work. That said, we stress that MIS* is still very useful in its current form when hydrodynamization happens first in the shear channel, since capturing the EHR response in the sound channel is more important in this case. This is what has been accomplished by MIS*.

3.4 Discussion on the extension of hydrodynamics

We developed the MIS* theory to describe how the medium responds in the extended hydrodynamic regime (EHR), where the high-frequency sound mode still has a longer lifetime than other excitations. Our analysis above shows that this framework could describe high-frequency hydrodynamic mode in EHR (or at least part of it) with a minimum number of model parameters. This is not the only possible formalism with which to describe EHR. An alternative method is to include higher-order gradient terms in hydrodynamics, and the efficiency of doing so relies on the convergence of the gradient expansion, which has attracted many recent studies [33–35]. See also ref. [36] for a different strategy in extending hydrodynamics.

In MIS*, π_1, π_2 are introduced to describe sound dispersion outside the hydrodynamic regime. While including non-hydrodynamic fields to extend hydrodynamic is not new and has been widely discussed in literature [37–39], most of those studies are motivated by the expectation that the number of relevant modes increases at shorter time scales or non-hydrodynamic distances. Moreover, the emergence of parametrically slow modes also necessitates including additional modes even in the hydrodynamic regime, and the result theory is referred to as "Hydro+" in ref. [40]. One familiar situation is near a critical point; the relaxation time of the fluctuations of the order parameter field grows with increasing correlation length. In all cases discussed above, the number of relevant modes is larger than that of hydrodynamic ones, which are conserved densities. In contrast, the number of slow

---

[4]In many references, "hydrodynamization" refers to the case when the bulk evolution is described by viscous hydrodynamics.

modes in EHR is the same as that of hydrodynamic ones in the sound channel. The purpose of including non-hydrodynamic dynamic fields $\pi_{1,2}^{\mu\nu}$ is not because they are additionally slow modes but because they bring about new parameters needed to characterize the dispersion of high-frequency sound modes.[5] This distinguishes the MIS* theory from early studies.

4 Perturbation in medium undergoing Bjorken expansion

In this section, we will study the energy-momentum response around a Bjorken expanding conformal plasma and compare the results with those in the static background.

4.1 Response function for Bjorken background

We divide the stress-energy tensor (EMT) into a background and a perturbation part:

$$T^{\mu\nu}(\tau, \boldsymbol{x}) = T_0^{\mu\nu}(\tau) + \delta T^{\mu\nu}(\tau, \boldsymbol{x}), \tag{4.1}$$

where we assume the background is under Bjorken expanding. Accordingly, background EMT $T_0^{\mu\nu}(\tau)$ only depends on the Bjorken proper time $\tau = \sqrt{t^2 - z^2}$ and takes form

$$T_0^{\mu\nu} = \mathrm{diag}\left(\epsilon_0, P_0, P_0, P_0\right) + \mathrm{diag}\left(0, 1, 1, -\frac{2}{\tau^2}\right) \pi_0. \tag{4.2}$$

Here, the first and second terms on the R.H.S. of eq. (4.2) represent the contribution from the ideal and non-equilibrium part of the constitutive relation, see eq. (2.39). The background $\pi_0^{\mu\nu}$ is diagonalized and is fully parameterized by $\pi_0 = \pi_0^{xx} = \pi_0^{yy}$ for a conformal system under consideration.

Following ref. [41], we define the response function describing the subsequent evolution of the initial perturbation $\delta T^{\mu\nu}$ at $(\tau', \boldsymbol{x}'_\perp)$ (cf. eq. (2.1)):

$$\delta T^{\mu\nu}(\tau, \boldsymbol{x}_\perp) = \int d^2\boldsymbol{x}'_\perp \, \mathcal{G}^{\mu\nu}{}_{\alpha\beta}(\boldsymbol{x}_\perp - \boldsymbol{x}'_\perp; \tau, \tau') \, \delta T^{\alpha\beta}(\boldsymbol{x}'_\perp, \tau'). \tag{4.3}$$

where we have used the fact that the response functions depend only on the different $\boldsymbol{r} = \boldsymbol{x}_\perp - \boldsymbol{x}'_\perp$. For the present purpose, we only consider the perturbation that depends on the spatial vector lying entirely in the plane transverse to z-direction $\boldsymbol{x}_\perp$. The non-zero independent components of $\delta T^{\mu\nu}$ are

$$\delta\epsilon = \delta T^{\tau\tau} \qquad \delta g^a \equiv \delta T^{\tau a}, \qquad \delta T^{ab}, \tag{4.4}$$

where $a = x, y$ and δg^a is nothing but transverse momentum density perturbation. The value of $\delta T^{\eta\eta}$ is related to $\delta\epsilon, \delta T^{ab}$ by the conformality condition. We are interested in the response of the plasma near equilibrium, so we shall implicitly assume that τ' is larger than the thermalization time of the plasma. The response functions of a far-from-equilibrium Bjorken expanding plasma have been studied using effective QCD kinetic theory [41–43] and RTA kinetic theory [44].

---

[5]In our view, to understand the need to introduce non-hydrodynamic d.o.fs. $\pi_{1,2}^{\mu\nu}$ in MIS*, it might be useful to recall that some heavy particles are introduced to make neutrino light through the sea-saw mechanism in some beyond-standard model scenarios.

Following the discussion of ref. [41], one can show that there are five independent components of $\mathcal{G}^{\mu\nu}{}_{\alpha\beta}$ that describe the energy-momentum response to the initial energy density $\delta\epsilon$ and initial transverse momentum density δg^a disturbance (see also ref. [44]):

$$\mathcal{G}^{\tau\tau}{}_{\tau\tau}(\boldsymbol{r}) \equiv \mathcal{G}_{\epsilon\epsilon}(r)\,, \tag{4.5a}$$

$$\mathcal{G}^{\tau a}{}_{\tau\tau}(\boldsymbol{r}) \equiv \hat{r}^a\,\mathcal{G}_{\epsilon L}(r) \qquad \mathcal{G}^{\tau\tau}{}_{\tau a}(\boldsymbol{r}) \equiv \hat{r}^a\,\mathcal{G}_{L\epsilon}(r)\,, \tag{4.5b}$$

$$\mathcal{G}^{\tau a}{}_{\tau b}(\boldsymbol{r}) = \hat{r}^a\hat{r}^b\mathcal{G}_{LL}(r) + \left(\delta^{ab} - \hat{r}^a\hat{r}^b\right)\mathcal{G}_{TT}(r)\,. \tag{4.5c}$$

In the above expressions, we suppress the dependence on τ, τ' in R.F. to highlight their dependence on $\boldsymbol{r}$. The physical interpretation of those R.F. should be transparent. For example, $\mathcal{G}_{\epsilon L}$ describes energy density at τ induced by the momentum density disturbance projected along direction $\hat{r}$ at initial time τ'. Likewise, $\mathcal{G}_{TT}$ describes the transverse (with respect to $\hat{r}$) momentum density induced by the initial momentum density.

Following the common practice (see refs. [42–44]), we first compute $\mathcal{G}^{\mu\nu}{}_{\alpha\beta}$ in Fourier space $\boldsymbol{k} = (k_x, k_y)$ and obtain the real space R.F.

$$\mathcal{G}^{\mu\nu}{}_{\alpha\beta}(\boldsymbol{x} - \boldsymbol{x}_0; \tau, \tau_0) = \int \frac{d^2\boldsymbol{k}}{(2\pi)^2}\,\mathcal{G}^{\mu\nu}{}_{\alpha\beta}(\boldsymbol{k}; \tau, \tau_0)\,e^{i\boldsymbol{k}\cdot(\boldsymbol{x}-\boldsymbol{x}_0)}\,. \tag{4.6}$$

The relevant independent components of $G^{\mu\nu}{}_{\alpha\beta}(\boldsymbol{k}; \tau, \tau_0)$ are [41]

$$\mathcal{G}^{\tau\tau}{}_{\tau\tau}(\boldsymbol{k}) = \mathcal{G}_{\epsilon\epsilon}(\boldsymbol{k})\,, \tag{4.7}$$

$$\mathcal{G}^{\tau\tau}{}_{\tau a}(k) = i\,\hat{\boldsymbol{k}}_a\mathcal{G}_{\epsilon L}(k)\,, \qquad \mathcal{G}^{\tau a}{}_{\tau\tau}(\boldsymbol{k}) = i\,\hat{\boldsymbol{k}}_a\,\mathcal{G}_{L\epsilon}(k)\,, \tag{4.8}$$

$$\mathcal{G}^{\tau a}{}_{\tau b}(\boldsymbol{k}) = \hat{k}^a\hat{k}^b\,\mathcal{G}_{LL}(k) + (\delta^{ab} - \hat{k}^a\hat{k}^b)\,\mathcal{G}_{TT}(k)\,. \tag{4.9}$$

They determine the real-space response function through the relation:

$$\mathcal{G}_{\epsilon\epsilon}(r) = \int \frac{dk\,k}{2\pi}\,J_0(kr)\,\mathcal{G}_{\epsilon\epsilon}(k)\,, \tag{4.10a}$$

$$\mathcal{G}_{\epsilon L}(r) = \int \frac{dk\,k}{2\pi}\,J_1(kr)\mathcal{G}_{\epsilon L}(k)\,, \qquad \mathcal{G}_{L\epsilon}(r) = \int \frac{dk\,k}{2\pi}\,J_1(kr)\mathcal{G}_{L\epsilon}(k)\,, \tag{4.10b}$$

$$\mathcal{G}_{LL}(r) = \int \frac{dk\,k}{2\pi}\frac{1}{2}\left[(J_0(kr) - J_2(kr))\,\mathcal{G}_{LL}(k) + (J_0(kr) + J_2(kr))\,\mathcal{G}_{TT}(k)\right]\,, \tag{4.10c}$$

$$\mathcal{G}_{TT}(r) = \int \frac{dk\,k}{2\pi}\frac{1}{2}\left[(J_0(kr) + J_2(kr))\,\mathcal{G}_{LL}(k) + (J_0(kr) - J_2(kr))\,\mathcal{G}_{TT}(k)\right]\,, \tag{4.10d}$$

where $J_{0,1,2}$ are standard Bessel functions.

4.2 Kinetic theory calculation

In this section, we present the calculation of the response function for a Bjorken expanding plasma using RTA kinetic equation (2.16). In Bjorken coordinate the kinetic equation (2.16) reads

$$\frac{\partial f}{\partial \tau} + \frac{\mathbf{p}_a}{p}\frac{\partial f}{\partial x_a} - \frac{p^\eta}{\tau}\frac{\partial f}{\partial p^\eta} = -\frac{p_\mu u^\nu\,(f - f_{\rm eq})}{p\,\tau_R} \tag{4.11}$$

where the summation over the dummy variable a is understood. As explained earlier, we consider massless particles with single-particle energy $p = |\boldsymbol{p}|$.

Since we are interested in energy-momentum disturbance, it is convenient to introduce the integrated distribution function (see also refs. [45, 46])

$$F(\hat{\boldsymbol{p}}) = \int_0^\infty \frac{dp}{2\pi^2} p^3 f \,, \tag{4.12}$$

from which one can obtain the components of EMT through the solid angle integration with the appropriate weight, e.g.,

$$\epsilon = \int \frac{d\Omega}{4\pi} F, \qquad g_a = \int \frac{d\Omega}{4\pi} \frac{p_a}{p} F \,, \qquad T_{ab} = \int \frac{d\Omega}{4\pi} \left(\frac{p_a p_b}{p}\right) F \,. \tag{4.13}$$

By performing the integration over dp over the kinetic equation (4.11), we then derive the equation for F (see also refs. [4, 45, 47])

$$\left[\partial_\tau + \hat{p}_a \frac{\partial}{\partial x_a} + \frac{1}{\tau}\left(4\cos^2\theta - \cos\theta(1-\cos^2\theta)\,\partial_{\cos\theta}\right)\right] F = -\frac{1}{\tau_R} \int_0^\infty \frac{dp}{2\pi^2} p^2 \,(p\cdot u)\,(f - f_{\rm eq}) \,. \tag{4.14}$$

We first consider background solution $F_0(\tau, \cos\theta)$ with $u_0^\mu = (1, 0, 0, 0)$ (in Bjorken coordinate). The equation (4.14) reduces to

$$\left[\partial_\tau + \frac{1}{\tau}\left(4\cos^2\theta - \cos\theta(1-\cos^2\theta)\,\partial_{\cos\theta}\right)\right] F_0(\tau, \cos\theta) = \frac{1}{\tau_R}\left[\epsilon_0(\tau) - F_0(\tau, \cos\theta)\right] \,. \tag{4.15}$$

The R.H.S. of eq. (4.15) can be understood from the fact that in equilibrium, $F_0 = \epsilon_0$ and is independent of $\cos\theta$.

Next, we turn to the perturbation around the background solution $F = F_0 + \delta F$. Linearizing the L.H.S. of eq. (4.14) is straightforward. For the R.H.S., we have

$$\frac{1}{p}\delta\left[\frac{p\cdot u}{\tau_R}(f - f_{\rm eq})\right] = \frac{\delta f - \delta f_{\rm eq}}{\tau_{R,0}} + \left(p\cdot\delta u - \frac{p^0\,\delta\tau_R}{\tau_R}\right)\frac{f_0 - f_{\rm eq,0}}{\tau_{R,0}} \,. \tag{4.16}$$

Note $\delta\tau_R$ term will be present because τ_R depends on ϵ (see eq. (2.19)). For convenience, we shall count $f_0 - f_{\rm eq,0}$ of the order $\mathcal{O}(\delta_0)$ where δ_0 is assumed to be another small parameter as we are interested in the near equilibrium background. In fact, $\pi_0/w_0 \sim \mathcal{O}(\delta_0)$ in this counting scheme. For a simple estimate of this ratio, we use the first-order hydrodynamic expectation $\pi_0/w_0 = 2\eta/(3\tau w)$. Using $\eta/w = (1/5)\tau_R$ in the RTA kinetic theory (2.54), we find $\pi_0/w_0 \leq 2/15$ for $\tau > \tau_R$ and is numerically small. See also figure 5 where the numerical solutions to the background equation (4.15) is plotted and the smallness of π_0/w_0 is verified. To further simplify our analysis, we will ignore the terms of the order $\mathcal{O}(\delta_0\,\delta)$, i.e. the second term on the R.H.S of eq. (4.16).

To calculate the first term on the R.H.S of eq. (4.16), one can use an expression analogous to eq. (2.21) to expand $\delta f_{\rm eq}$. On the other hand,

$$\delta T^{\tau a} = \delta g^a = w_0 \delta u^a + \delta\pi^{\tau a} \,, \tag{4.17}$$

and $\pi^{\mu\nu}$ is transverse to the fluid velocity

$$\delta u_\mu \pi_0^{\mu\nu} + u_\mu \delta\pi_0^{\mu\nu} = 0 \,, \tag{4.18}$$

so we find $\delta\pi^{\tau a} = \pi_0\delta u^a$ and consequently

$$\delta u^a = \frac{g^a}{w_0(1 - \frac{\pi_0}{w_0})} = \frac{g^a}{w_0} + \mathcal{O}(\delta\,\delta_0)\,. \tag{4.19}$$

After integrating the linearized kinetic equation over $\int_0^\infty dp\,p^2$, we obtain, in Fourier space, the equation for δF (see also ref. [47])

$$\left[\partial_\tau + i\,k_a\,p_a + \frac{1}{\tau}\left(4\cos^2\theta - \cos\theta(1 - \cos^2\theta)\,\partial_{\cos\theta}\right)\right]\delta F = \frac{1}{\tau_R}\left(\delta\epsilon + \frac{1}{c_s^2}\delta g^a \cdot \hat{p} - \delta F\right)\,. \tag{4.20}$$

By solving eq. (4.20), we can obtain the response function through the definition in section 4.1.

4.3 Hydrodynamic theory calculation

As we did in the previous sections 2.3, we collectively call first-order hydrodynamics, MIS (or its variants), and MIS* "hydrodynamic theories".

We shall first derive E.o.M for background energy density ϵ_0 and linearized energy and momentum density $\delta\epsilon, \delta g^a$. The resulting equations apply equally to all "Hydrodynamic theories" under consideration. In contrast, the description of $\pi^{\mu\nu}$ differs among those theories and will be specified later.

We begin with the energy-momentum conservation equation

$$\nabla_\mu T^{\mu\nu} = \partial_\mu T^{\mu\nu} + \Gamma^\mu_{\mu\lambda}T^{\lambda\nu} + \Gamma^\nu_{\mu\lambda}T^{\mu\lambda}\,, \tag{4.21}$$

where the non-zero connection in Bjorken coordinates are $\Gamma^\eta_{\eta\eta} = \tau, \Gamma^\eta_{\eta\tau} = \Gamma^\eta_{\tau\eta} = 1/\tau$. Using the expression for the background EMT (4.2), we obtain

$$\partial_\tau\epsilon_0 = -\frac{4}{3\tau}\epsilon_0 + \frac{2\pi_0}{\tau}\,, \tag{4.22}$$

Turning to the perturbation, we have from (4.21) that

$$\left(\partial_\tau + \frac{4}{3\tau}\right)\delta\epsilon + \partial_a\delta g^a - \tau\,\delta\pi^{\eta\eta} = 0\,, \tag{4.23a}$$

$$\left(\partial_\tau + \frac{1}{\tau}\right)\delta g^a + \frac{1}{3}\partial^a\delta\epsilon + \partial_b\delta\pi^{ba} = 0\,, \tag{4.23b}$$

where we have used eq. (4.4).

Now, we turn to discuss $\pi_0^{\mu\nu}, \delta\pi^{\mu\nu}$ for different "hydrodynamic theories". As discussed earlier, the background $\pi_0^{\mu\nu}$ is fully determined by π_0. To close eqs. (4.23), only $\delta\pi^{ab}$ are needed since $\delta\pi^{\eta\eta}$ can be expressed in terms of $d\pi^{ab}$ due to the conformality condition, i.e.,

$$\delta\pi^{\eta\eta} = -\frac{1}{\tau^2}\sum_a \delta\pi^{aa}\,. \tag{4.24}$$

In the first-order hydrodynamics, $\pi^{\mu\nu}$ is not dynamical and (2.41) yields

$$\pi_0 = -2\eta_0\,\sigma_0^{\mu\nu}\,, \qquad \delta\pi^{\mu\nu} = -2\eta_0\delta\sigma^{\mu\nu}\,. \tag{4.25}$$

where for the background

$$\sigma_0^{\mu\nu} = \frac{1}{3\tau}\text{diag}\left\{0, -1, -1, \frac{2}{\tau^2}\right\}. \tag{4.26}$$

Further using eq. (4.19), we arrived at the expression:

$$\delta\sigma^{ab} = \frac{1}{w_0}\,\partial^{\langle a}\,\delta g^{b\rangle}\,. \tag{4.27}$$

Following ref. [48], we shall use a modern variant of MIS, i.e. the theory formulated by Denicol, Niemi, Molnar and Rischke (DNMR) [49] where the equations of motion for $\pi^{\mu\nu}$ reads (see ref. [24] for examples of other variants of the second-order hydrodynamic theories):

$$D\pi^{\mu\nu} = -\frac{\pi^{\mu\nu} + 2\eta\sigma^{\mu\nu}}{\tau_\pi} - \frac{4}{3}\pi^{\mu\nu}\theta - \tilde{\lambda}_1\pi_\alpha^{\langle\mu}\sigma^{\nu\rangle\alpha} - \dots. \tag{4.28}$$

Here, ... on the L.H.S of (4.28) denotes a term proportional to the vorticity, but we shall discard this contribution since the Bjorken flow is irrotational. The second-order transport coefficient equals $\tilde{\lambda}_1 = 10/7$ by matching to RTA kinetic theory [48].

The DNMR equation for the background reads [48]

$$\partial_\tau\pi_0 = -\frac{1}{\tau_\pi}\left(\pi_0 - \frac{2\eta}{3\tau}\right) - \left(\frac{4}{3} + \frac{\tilde{\lambda}_1}{3}\right)\frac{\pi_0}{\tau} \tag{4.29}$$

and the linearized equation can be written as

$$\partial_\tau\delta\pi^{ab} = -\frac{\delta\pi^{ab} + 2\eta\delta\sigma^{ab}}{\tau_\pi} + \frac{4}{3\tau}\delta\pi^{ab} + \mathcal{O}(\delta_0\delta)\,. \tag{4.30}$$

Here and hereafter, we shall drop the terms of the order $\mathcal{O}(\delta_0\delta)$ as we have already done in kinetic theory calculations.

Finally, we discuss the MIS* theory introduced in section 3.2 in the limit $\tau_2/\tau_1 \to 0$ such that $\pi_2^{\mu\mu}$ (see eq. (3.5)) is given by

$$\pi_2^{\mu\nu} = -2\eta_2\sigma^{\mu\nu}\,. \tag{4.31}$$

For $\pi_1^{\mu\nu}$, instead of using (3.6), we consider the equation of the form (4.28), i.e.,

$$\pi^{\mu\nu} = \pi_1^{\mu\nu} + \pi_2^{\mu\nu}, \tag{4.32}$$

$$D\pi_1^{\mu\nu} = -\frac{\pi^{\mu\nu} + 2\eta_1\sigma^{\mu\nu}}{\tau_1} - \frac{4}{3}\pi_1^{\mu\nu}\theta - \tilde{\lambda}_1\pi_\alpha^{\langle\mu}\sigma^{\nu\rangle\alpha} \tag{4.33}$$

so that when $\eta_2 = 0$, our theory reduces to eq. (4.28). Consequently, the background and linearized equation for $\pi_1^{\mu\nu}$ can be obtained by replacing $\pi_0, \delta\pi^{ab}, \eta$ etc in eqs. (4.29), (4.30). with $(\pi_1)_0, \delta\pi_1^{ab}, \eta_1$ respectively.

5 Results for Bjorken expansion

5.1 Initial condition

We begin the background evolution at $\tau \geq \tau_R(\epsilon(\tau))$ when the system is expected to be near equilibrium. Because of the conformality of the system under consideration, the solutions to eq. (4.15) and (4.20) only depend on the rescaled time τ/τ_R. Instead of specifying the overall normalization in $\tau_R \propto \epsilon^{-1/4}$, we first define τ_0 such that $\tau_0 = \tau_R(\epsilon_{\rm in})$ for a given $\epsilon_{\rm in}$. We then use τ_0 to set up the temporal scale and present results in terms of τ/τ_0 or τ/τ_R. By construction, the background evolution starts at $\tau/\tau_0 = 1$

Since the background evolution of "hydrodynamic theories" is fully determined by the initial values of energy density $\epsilon_{\rm in}$ and that of π_0, denoted by $\pi_{\rm in}$, we require the initial profile of F is also fully specified by $\epsilon_{\rm in}, \pi_{\rm in}$ to facilitate a comparison. According to eq. (4.13), we use the parameterization:

$$F_{\rm in}(\cos\theta) = \epsilon_{\rm in} + \frac{15}{4}(1 - \cos^2\theta)\,\pi_{\rm in}\,. \tag{5.1}$$

We use the same $\epsilon_{\rm in}, \pi_{\rm in}$ for the first order and MIS theory. For MIS*, the dynamical field is $\pi_1^{\mu\nu}$ and will be initialized as $\pi_1^{\mu\nu}(\tau_0) = (1 - \delta)\pi_{\rm in}$.

After obtaining the background evolution, we then turn on initial energy disturbance $\delta\epsilon_{\rm in}$ (or momentum density $g_{\rm in}^x, g_{\rm in}^y$) at $\tau' = 2\tau_0$. Correspondingly, we set $\delta F(\theta) = \delta\epsilon_{\rm in}$ (or $\delta F(\theta) = \delta g_{\rm in}^x \sin\theta\cos\phi, \delta g_{\rm in}^y \sin\theta\sin\phi$) to solve the linearized kinetic equation (4.20). The same values of initial hydrodynamic fields are used to solve linearized "hydrodynamic theories".

We close this subsection by noting that the rescaled solution $\epsilon_0/\epsilon_{\rm in}, \pi_0/\epsilon_{\rm in}$ as well as the rescaled response function do not depend on the magnitude of $\epsilon_{\rm in}$ and $\delta\epsilon_{\rm in}, g_{\rm in}^a$. Therefore, we shall not set their values in practice but simply present results in terms of rescaled quantities.

5.2 Background solution

To determine the background evolution in different theories, we have solved the corresponding equations derived in section 4.2 and section 4.3. In figure 5 we plot the dimensionless ratio $\epsilon_0(\tau)/(\epsilon_{\rm in}(\tau_0/\tau)^{4/3}))$ (left) and $\pi_0(\tau)/w_0(\tau)$ (right) as a function of the rescaled proper time $\tau/\tau_R(\epsilon)$ for kinetic, DNMR and MIS* theories. For definiteness, MIS* results are obtained with the choice of MIS parameters $(\delta, \gamma) = (0.2, 0.8)$, as motivated by figure 3. The solid and dashed curves correspond to $\pi_{\rm in}/w_{\rm in} = 0$ and $\pi_{\rm in}/\epsilon_{\rm in} = 3/4$ respectively. We observe differences among different theories in the background evolution are within a few percent. This indicates that if we see any significant difference in response functions, it is mainly due to the discrepancy in their description of the response. Finally, figure 5 (right) where π_0/w_0 is plotted, we confirm that this ratio is indeed small, as we claimed earlier. We also notice that background evolution is insensitive to the choice of $\pi_{\rm in}/w_{\rm in}$ and we shall compute the response function for $\pi_{\rm in}/w_{\rm in}$.

5.3 Response in Fourier space

The functions defined in eq. (4.5) describe the energy and momentum density distribution at τ caused by the energy-momentum perturbation at τ' for a Bjorken expanding plasma. Figure 6 compares $G_{\epsilon\epsilon}, G_{\epsilon L}, G_{TT}$ in spatial Fourier space in RTA kinetic theory (black curves)
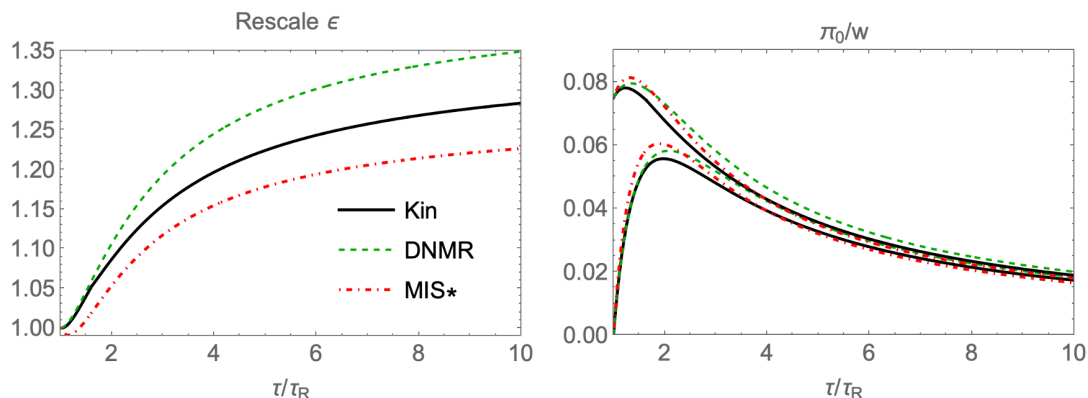
Figure 5. Left: background solution with $\pi_{\text{in}}/w_{\text{in}} = 0$ for rescaled energy density $\epsilon(\tau)/(\epsilon_{\text{in}}(\tau_0/\tau)^{4/3})$ from different "hydrodynamics theories" as compared to RTA solution. Right: the evolution of π_0/w. The upper and lower curves correspond to the solutions with $\pi_{\text{in}}/w_{\text{in}} = 0$ and $\pi_{\text{in}}/w_{\text{in}} = 0.75$ respectively.

with those in "hydrodynamic theories". When solving MIS*, we use the same range of δ, γ that gives a reasonable description of the RTA sound propagation in EHR. For better visualization, we rescale the response functions by multiplying $(\tau/\tau')^a$ so that their magnitudes are of the order of unity. The scaling exponent $a = 4/3$ for $\mathcal{G}_{\epsilon\epsilon}$ and $a = 1$ for the others, guided by the evolution of the background energy and momentum density for ideal hydrodynamics, which behave as $\tau^{-4/3}$ and τ^{-1} respectively. We present results with three representative values of $\Delta\tau = \tau - \tau'$, i.e. $\Delta\tau = 2, 8, 16\tau_0$ in figure 6. Those plots reiterate that neither first-order nor MIS theory describes the response beyond the small gradient regime, while MIS* significantly improves the description to a larger gradient domain. Meanwhile, $\mathcal{G}_{TT}(k)$, corresponding to the shear channel, "hydrodynamizes" at a smaller value of $\Delta\tau$ as compared with other response functions. This further emphasizes the significance of describing sound propagation for response at a non-hydrodynamic time scale.

When comparing the energy-energy response function $\mathcal{G}_{\epsilon\epsilon}$ and the transverse momentum density response function $\mathcal{G}_{TT}$ to their counterparts for the static background (i.e., G^L, G^T in figure 4), an interesting observation can be made. The responses in both backgrounds are qualitatively similar and semi-quantitatively comparable. This can be explained by considering a fluid background with a characteristic size of in-homogeneity l_* (This scale in a heavy-ion collision has been estimated in ref. [50]). For gradients at $k > 1/l_*$, including those living in the EHR, the response cannot resolve the long-wavelength structure of the background. Consequently, the EHR response should be insensitive to the difference in the background profile.

To better understand the preceding point, we simplify the first equation in eq. (4.23) under the limit $k\tau > 1$.

$$\partial_\tau \delta\epsilon + \partial_a \delta g^a = 0 \,. \tag{5.2}$$

This equation is the same as the linearized energy conservation equation in the static background upon replacing the Bjorken time τ with t. Consequently, the response function for those two different backgrounds should be comparable. Moreover, this also implies that
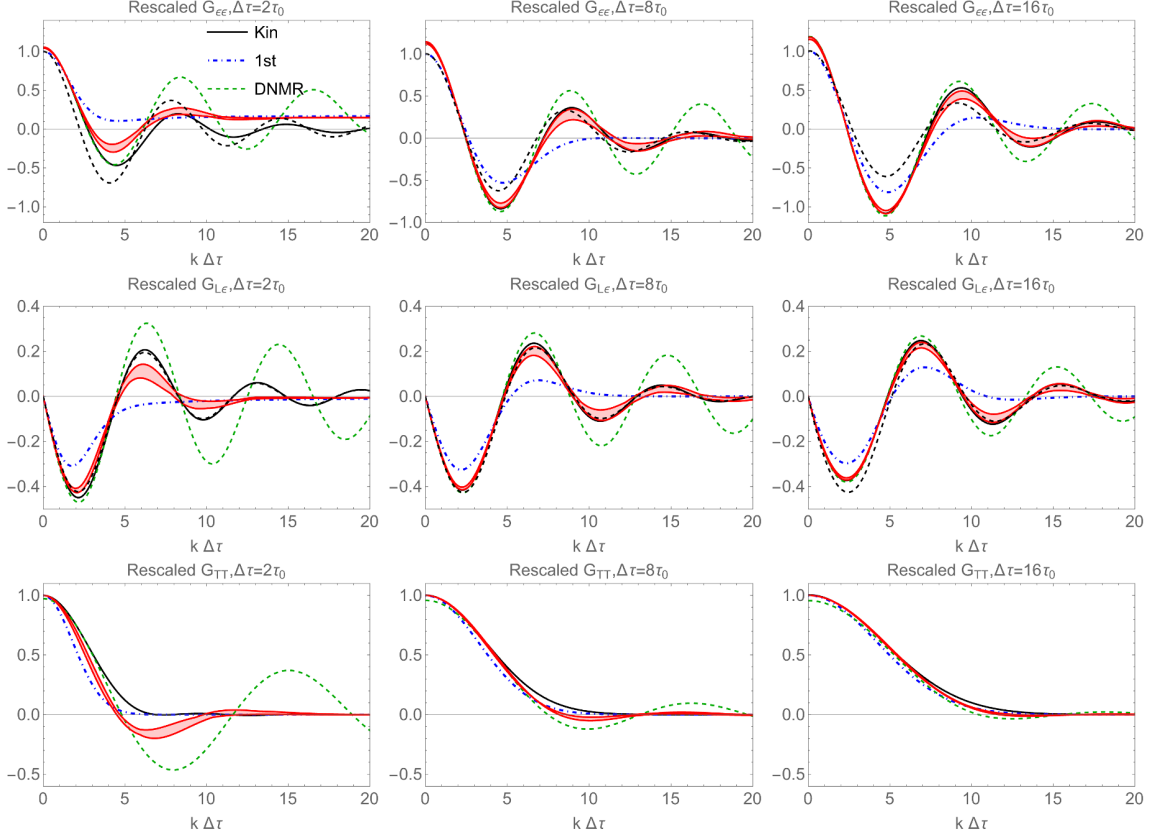
Figure 6. The energy-momentum response function $G_{\epsilon\epsilon}$, $G_{L\epsilon}$, G_{TT}, defined in eqs. (4.6) and (4.7) (cf. their analogs in the static background in figure 6), are plotted in the solid black curves from the first to the third row as a function of $k\Delta\tau$. Those functions are rescaled by multiplying $(\tau/\tau')^{4/3}$, (τ/τ'), (τ/τ') respectively, see text. The results of RTA kinetic theory, first-order hydrodynamics, and MIS theory are shown in the solid, dotted, and dashed curves, respectively. The MIS* results are plotted as red bands, computed from $0.2 < \delta < 0.3$, $0.7 < \gamma < 0.8$. Three values of $\Delta\tau$ represent the response function at an early, intermediate, and late time (from left to right). To test relation (5.3), we plot $(\tau/\tau')G_{LL}$ and $(\tau/\tau')G_{\epsilon L}/3$ from the kinetic theory in the black dashed curve in the first and second row, respectively. They are to be compared with rescaled $G_{\epsilon\epsilon}$ and $G_{L\epsilon}$.

in this regime, the number of independent R.F. for the expanding background can be further reduced, as there are only two in energy-momentum response in static background. Indeed, we found in figure 6 that for Bjorken expansion, the following relation, which can be derived by taking $k\tau \gg 1$ limit, holds approximately

$$\left(\frac{\tau}{\tau_0}\right)^{4/3} G_{\epsilon\epsilon} \approx \frac{\tau}{\tau_0} G_{LL} \qquad G_{L\epsilon} \approx \frac{1}{3} G_{\epsilon L} \,. \tag{5.3}$$

5.4 Response in real space

We obtain the real space response function by taking the Fourier transforming according to eq. (4.6) where a smearing function $e^{-k^2/(2k_{\rm UV}^2)}$ in its integrand is included to eliminate contributions from high values of k. Introducing this UV cut-off is a common practice in previous studies [41], and is necessary for several reasons. Firstly, we are interested in the
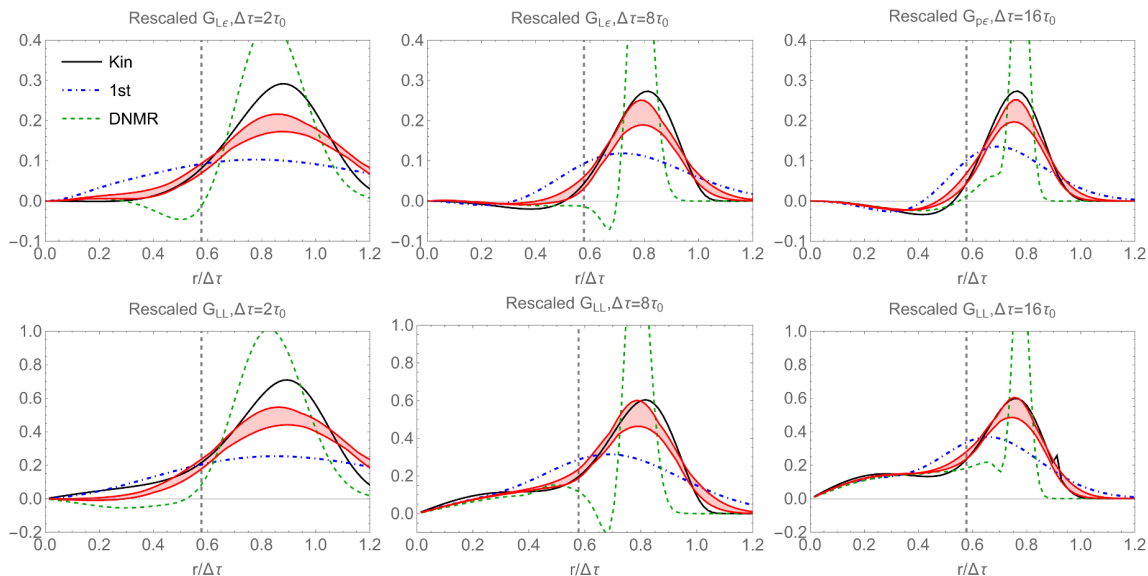
Figure 7. The same as figure 6 but for the real-space response function $G_{L\epsilon}, G_{LL}$ (defined in eq. (4.5)) v.s $r/\Delta\tau$ for the Bjorken expanding plasma. The vertical dashed black lines correspond to the value of conformal sound velocity $c_s = \sqrt{1/3} \approx 0.577$.

response in EHR, which in general may not include arbitrarily large values of k Secondly, the kinetic theory is invalid when the gradient is larger than the typical effective temperature, as the mixing between particle and anti-particle can not be ignored in such cases. Thirdly, in many physics situations, the source of energy-momentum perturbation should only have finite support in the k-space. In practice, we use $k_{\rm UV} = 3/\tau_0$ and have checked the results shown below are insensitive to the choice of $k_{\rm UV}$ as long as $k_{\rm UV} \gg \tau_0$.

In figure 7, we have graphed the rescaled response function $\mathcal{G}_{L\epsilon}, \mathcal{G}_{LL}$ against $r/\Delta\tau$ for the same set of values of $\Delta\tau$ as we did in figure 6 (see ref. [1] for $\mathcal{G}_{\epsilon\epsilon}$). For causality to hold, R.F. must disappear outside the causal circle $r/\Delta\tau \leq 1$. Due to the smearing function we introduce, the numerical real space R.F. might be non-zero outside the causal circle, but it will be of a small magnitude.

The most important qualitative feature of the real space R.F. associated with energy and momentum response (e.g., $\mathcal{G}_{L\epsilon}$ in the first row of figure 7) is the presence of a peak at a specific value of $v_{\rm eff} = r/\Delta\tau$. This value represents the effective velocity for the propagation of energy and momentum perturbation. The real space results are given by summing the contribution from different k with an appropriate weight. Therefore $v_{\rm eff}$ also tells us the average phase velocity of the sound. As time passes, $v_{\rm eff}$ approaches the hydrodynamic limit $c_s = 1/\sqrt{3}$ at late times. However, even at $\Delta\tau = 16\tau_R$, $v_{\rm eff}$ is still visually different from c_s. Going back in time, $v_{\rm eff}$ is supersonic and becomes closer to 0.86, the maximum value of the sound velocity in EHR (see figure 3). This indicates that unless $\Delta\tau$ is very large, the contribution from EHR is significant, and high-frequency sound mode plays a crucial role in early times.

Regarding the peak's width, it measures the average sound attenuation rate, where a larger attenuation rate implies a broader peak. We anticipate from figure 3 and now confirm here that first-order theory (MIS/DNMR) will underestimate (overestimate) the

peak width. In contrast, MIS* theory reasonably describes almost all the R.F. functions under consideration with a suitable model parameter δ, γ. This confirms that MIS* can be utilized to describe the response in the EHR.

Finally, we note that $\mathcal{G}_{LL}(r)$, defined in relation (4.10) and shown in the second row of figure 7, receive contributions from both sound and shear modes, but it exhibits the sound peak in $r/\Delta\tau$ as its main feature. We have also checked that this peak is also in $\mathcal{G}_{TT}$. This further makes us believe that describing non-hydrodynamic sound propagation is more important than that for the shear mode.

6 Non-hydrodynamic response from the Euclidean correlators

In this section, we discuss the implications of the EHR scenario for extracting the real-time properties of QGP from Euclidean correlators, which are directly accessible from first-principle lattice QCD calculations.

We recall the relation between Euclidean correlator G_E and the spectral density ρ:

$$G_E(\tau_E, k) = \int_0^\infty d\omega \rho(\omega, k) \frac{\cosh \omega \left(\tau_E - \frac{1}{2T} \right)}{\sinh \frac{\omega}{2T}} . \tag{6.1}$$

where τ_E is the Euclidean time. There have been extensive efforts in extracting the low-frequency behavior of spectral density from the lattice QCD calculation of G_E to determine transport coefficients such as shear viscosity non-perturbatively (see ref. [51] for a review). Nevertheless, since the characteristic frequency of the kernel that is convoluted with the spectral density in eq. (6.1) is of the order $\omega_T = \pi T$, the resulting Euclidean correlators are notoriously insensitive to the features in hydrodynamic regimes where the typical gradient and frequency are expected to be smaller than ω_T.

Here, we argue that the characteristic gradient/frequency in the conjectured EHR of QGP should be of the order ω_T — a frequency domain to which the Euclidean correlator may still be sensitive. To support our claim, we consider the rescaled wave momentum $\tilde{k} = \frac{k}{(s/\eta)Tc_s^2}$. While η/s can be different even by order of magnitude for different microscopic theories, we hope that the dimensionless value of the characteristic $\tilde{k}$ in EHR, $\tilde{k}_{\mathrm{EHR}}$, is of the same order in those theories. In fact, the study of ref. [27] indeed indicates that the retarded correlator expressed in terms of $\tilde{k}$ is much less sensitive to the microscopic details. For RTA kinetic theory, we can use eq. (2.54) and read from figure 3 that $\frac{9}{16} < \tilde{k} < \frac{9}{4}$ may be considered as the domain of EHR. In ref. [10], the spectral density of EMT has been calculated using the leading log Boltzmann equation for the QCD plasma. In sound channel, the authors observe that while hydrodynamics ceases to be a good description for $\tilde{k} > 0.7$, the peak associated with high-frequency sound (in the view of the present paper) in the spectral density persists up to $\tilde{k} \sim 5.6$ (see figure 2 of ref. [10]). On the other hand, for the SYM correlator obtained from the AdS/CFT method, the EHR exists for $\tilde{k} > 1$. Combining all the information above, it is reasonable to assume that for QGP, $\tilde{k}_{\mathrm{EHR}} = 1$–2, or

$$k_{\mathrm{EHR}} = (1\text{–}2) \left(\frac{\eta}{s} \right)^{-1} c_s^2 T . \tag{6.2}$$

Taking $\eta/s = 2 \times (1/4\pi)$ as a crude estimate for QGP gives $k_{\mathrm{EHR}} \sim \pi T$.

We now investigate the sensitivity of the Euclidean correlator G_E to the properties of EHR. For definiteness, we consider the energy-energy Euclidean correlator so that spectral density is given by $\rho = -\text{Im}G_R^{00,00}/\pi$. Motivated by refs. [52, 53], we assume a very simple EHR plus tree-level ansatz for the spectral function

$$\rho(\omega, k) = \rho_{\text{EHR}}(\omega, k)\theta(k - \omega) + \rho_{\text{tree}}(\omega, k)\theta(\omega - k)\,, \tag{6.3}$$

Here, ρ_{EHR} can be obtained by computing G_R from the MIS* response function through the relation (2.10). We find

$$\rho_{\text{EHR}}(\omega, k) = \frac{-1}{\pi}\text{Im}\left[\frac{wk^2}{\omega^2 - c_s^2 k^2 + i\nu(\omega)\omega k^2}\right]\,, \tag{6.4}$$

where we shall use the expression of $\nu(\omega)$ in MIS* (3.9), which we copy below for convenience

$$\nu(\omega) = \frac{4\nu_0}{3}\left(\frac{1 - \delta}{1 - i\omega\tau_1} + \delta\right)\,. \tag{6.5}$$

In the estimation below, we always use $w = \frac{3}{4}w_{SB} = \frac{1}{15}d_A\pi^2 T^4$ with $d_A = N_c^2 - 1$ and w_{SB} denotes the enthalpy density of a gluon plasma in Stefan-Boltzmann limit. The tree-level spectral function of a gluon plasma is taken from ref. [52]:

$$\rho_{\text{tree}}(\omega, k)\theta(\omega - k) = \frac{d_A k^4}{4(4\pi)^2}\int_0^1 dz\, \frac{(1 - z^2)^2\sinh\left(\frac{\omega}{2T}\right)}{\cosh\left(\frac{\omega}{2T} - \cosh\frac{kz}{2T}\right)}\,, \tag{6.6}$$

We have calculated the rescaled Euclidean correlator $\tilde{G}_E \equiv G_E/(d_A T^5)$ from eq. (6.3) for $k = (1/2, 1, 2, 4)\pi T$ at $\tau_E = \frac{1}{2T}$. The results will depend on parameters entering eq. (6.5), i.e. ν_0 (or η/s) and MIS* parameters τ_1, δ. We first perform the computation with the benchmark values $(\eta/s, \tau_1, \delta) = (1/2\pi, 4\eta/(sT), 0.1)$. Note that for SYM, $T\tau_\pi = 2.61(\eta/s)$ while a next leading order QCD calculation show $T\tau_\pi \approx 6.5(\eta/s)$ [54]. So we pick up a somewhat arbitrary value in between for τ_1 assuming τ_1 and τ_π should be of the same order. The value of δ is inspired by the comparison between high-frequency sound dispersion in MIS* theory and that in RTA kinetic theory and SYM theory [1]. Then we do the same but increase the value of one of the parameters by a factor of two to explore the sensitivity of G_E to those parameters.

The results shown in figure 8 are suggestive and encouraging. First, it confirms that at small k, the Euclidean correlator is insensitive to the value of the transport coefficient and MIS* parameters. For example, for $k = \frac{\pi T}{2}$ which might be considered as a gradient in the hydrodynamic regime, a factor of two difference in η/s only results in a few percent difference in G_E. On the other hand, as k increases, we observe sizable difference in G_E with varying MIS* parameters τ_1, δ. Furthermore, since the energy-energy response in EHR is determined by MIS* parameters together with η/s, we also observe the sensitivity of G_E to the value of shear viscosity at a non-hydrodynamic gradient. Those results suggest that by studying Euclidean correlators, we may be able to test the EHR scenario for QGP and could potentially extract both shear viscosity and parameters that characterize the medium's response in EHR.
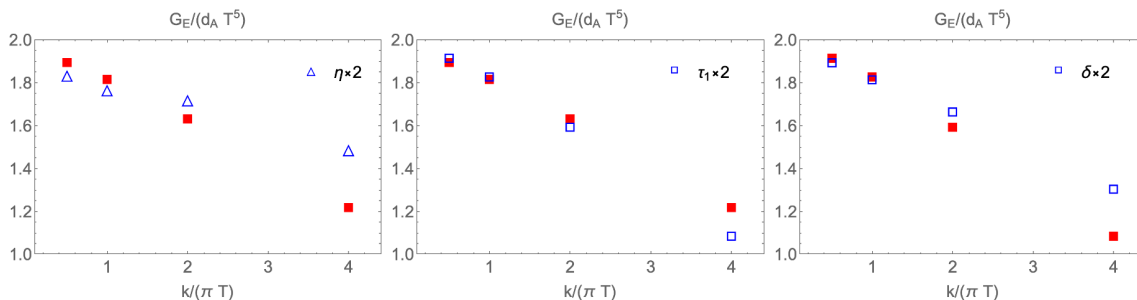
Figure 8. The rescaled Euclidean energy-energy retarded correlator G_E computed using eqs. (6.1) and (6.3) at Euclidean time $\tau_E = 1/(2T)$ for four different values of k. The filled squares show results obtained with the benchmark values of parameters in the parameterization of spectral density in the extended hydrodynamic regime, $(\eta/s, \tau_1, \delta) = (1/2\pi, 4\eta/(sT), 0.1)$. They are compared with G_E obtained from varying those parameters. See text.

7 Summary and outlook

We have studied the response of a QGP-like plasma to initial energy-momentum disturbance at a gradient outside the hydrodynamic regime. By comparing RTA kinetic theories results with those obtained from "hydrodynamic theories", we demonstrate a naive extrapolation of the first-order and second-order (or MIS/DNMR theory) outside hydrodynamic regime that fails to describe the response. Nevertheless, high-frequency sound modes might dominate the response at a non-hydrodynamic gradient. Under this extended hydrodynamic regime scenario, the description of the response can still be simplified significantly. Notably, we observe the significant improvement achieved by MIS* that we propose.

We have also compared the energy-momentum response function at static and Bjorken-expanding. We learned that at a non-hydrodynamic gradient, the response as a function of proper time is not very sensitive to the bulk background profile. This indicates that one may use the response functions obtained in the static background to estimate that in the expanding bulk profile, allowing for the simplification in the numerical studies. We also learned that although hydrodynamics would eventually describe those response functions, the "hydrodynamization time" of the response function would be numerically large. This, in turn, suggests that jet-medium observables might be employed to extract the medium's properties outside the hydrodynamic regime, and MIS* theory, or its extension, can be applied within this context.

We also hope the exploratory study presented in section 6 would arouse interest in extracting the medium's behavior at a non-hydrodynamic gradient from the lattice Euclidean correlator. The latter should be sensitive to the response at the gradient of order πT. This is precisely the key missing gap in our understanding of QGP's behavior.

by the LDRD Program at Los Alamos National Laboratory. When preparing for the draft, we used Grammaly-Go AI to improve the presentation.

References

[1] W. Ke and Y. Yin, *Does a Quark-Gluon Plasma Feature an Extended Hydrodynamic Regime?*, *Phys. Rev. Lett.* **130** (2023) 212303 [arXiv:2208.01046] [INSPIRE].

[2] F. D'Eramo, M. Lekaveckas, H. Liu and K. Rajagopal, *Momentum Broadening in Weakly Coupled Quark-Gluon Plasma (with a view to finding the quasiparticles within liquid quark-gluon plasma)*, *JHEP* **05** (2013) 031 [arXiv:1211.1922] [INSPIRE].

[3] F. D'Eramo, K. Rajagopal and Y. Yin, *Molière scattering in quark-gluon plasma: finding point-like scatterers in a liquid*, *JHEP* **01** (2019) 172 [arXiv:1808.03250] [INSPIRE].

[4] A. Kurkela, U.A. Wiedemann and B. Wu, *Flow in AA and pA as an interplay of fluid-like and non-fluid like excitations*, *Eur. Phys. J. C* **79** (2019) 965 [arXiv:1905.05139] [INSPIRE].

[5] J. Casalderrey-Solana, G. Milhano, D. Pablos and K. Rajagopal, *Modification of Jet Substructure in Heavy Ion Collisions as a Probe of the Resolution Length of Quark-Gluon Plasma*, *JHEP* **01** (2020) 044 [arXiv:1907.11248] [INSPIRE].

[6] A. Kurkela, A. Mazeliauskas and R. Törnkvist, *Collective flow in single-hit QCD kinetic theory*, *JHEP* **11** (2021) 216 [arXiv:2104.08179] [INSPIRE].

[7] Z. Yang, Y. He, I. Moult and X.-N. Wang, *Probing the Short-Distance Structure of the Quark-Gluon Plasma with Energy Correlators*, *Phys. Rev. Lett.* **132** (2024) 011901 [arXiv:2310.01500] [INSPIRE].

[8] A. Kurkela and U.A. Wiedemann, *Analytic structure of nonhydrodynamic modes in kinetic theory*, *Eur. Phys. J. C* **79** (2019) 776 [arXiv:1712.04376] [INSPIRE].

[9] M.P. Heller, A. Kurkela, M. Spaliński and V. Svensson, *Hydrodynamization in kinetic theory: Transient modes and the gradient expansion*, *Phys. Rev. D* **97** (2018) 091503 [arXiv:1609.04803] [INSPIRE].

[10] J. Hong and D. Teaney, *Spectral densities for hot QCD plasmas in a leading log approximation*, *Phys. Rev. C* **82** (2010) 044908 [arXiv:1003.0699] [INSPIRE].

[11] P. Romatschke, *Relativistic Fluid Dynamics Far From Local Equilibrium*, *Phys. Rev. Lett.* **120** (2018) 012301 [arXiv:1704.08699] [INSPIRE].

[12] R. Kunnawalkam Elayavalli and K.C. Zapp, *Medium response in JEWEL and its impact on jet shape observables in heavy ion collisions*, *JHEP* **07** (2017) 141 [arXiv:1707.01539] [INSPIRE].

[13] Y. He et al., *Interplaying mechanisms behind single inclusive jet suppression in heavy-ion collisions*, *Phys. Rev. C* **99** (2019) 054911 [arXiv:1809.02525] [INSPIRE].

[14] S. Cao and X.-N. Wang, *Jet quenching and medium response in high-energy heavy-ion collisions: a review*, *Rept. Prog. Phys.* **84** (2021) 024301 [arXiv:2002.04028] [INSPIRE].

[15] S. Cao and G.-Y. Qin, *Medium Response and Jet-Hadron Correlations in Relativistic Heavy-Ion Collisions*, *Ann. Rev. Nucl. Part. Sci.* **73** (2023) 205 [arXiv:2211.16821] [INSPIRE].

[16] JETSCAPE collaboration, *Hydrodynamic response to jets with a source based on causal diffusion*, *Nucl. Phys. A* **1005** (2021) 121920 [arXiv:2002.12250] [InSPIRE].

[17] J. Casalderrey-Solana, E.V. Shuryak and D. Teaney, *Conical flow induced by quenched QCD jets*, *J. Phys. Conf. Ser.* **27** (2005) 22 [hep-ph/0411315] [InSPIRE].

[18] R.B. Neufeld, B. Muller and J. Ruppert, *Sonic Mach Cones Induced by Fast Partons in a Perturbative Quark-Gluon Plasma*, *Phys. Rev. C* **78** (2008) 041901 [arXiv:0802.2254] [InSPIRE].

[19] J. Casalderrey-Solana et al., *Jet Wake from Linearized Hydrodynamics*, *JHEP* **05** (2021) 230 [arXiv:2010.01140] [InSPIRE].

[20] G.D. Moore and K.A. Sohrabi, *Kubo Formulae for Second-Order Hydrodynamic Coefficients*, *Phys. Rev. Lett.* **106** (2011) 122302 [arXiv:1007.5333] [InSPIRE].

[21] P. Petreczky and D. Teaney, *Heavy quark diffusion from the lattice*, *Phys. Rev. D* **73** (2006) 014508 [hep-ph/0507318] [InSPIRE].

[22] P.K. Kovtun and A.O. Starinets, *Quasinormal modes and holography*, *Phys. Rev. D* **72** (2005) 086009 [hep-th/0506184] [InSPIRE].

[23] P. Romatschke, *Retarded correlators in kinetic theory: branch cuts, poles and hydrodynamic onset transitions*, *Eur. Phys. J. C* **76** (2016) 352 [arXiv:1512.02641] [InSPIRE].

[24] R. Baier et al., *Relativistic viscous hydrodynamics, conformal invariance, and holography*, *JHEP* **04** (2008) 100 [arXiv:0712.2451] [InSPIRE].

[25] S. Bhattacharyya, V.E. Hubeny, S. Minwalla and M. Rangamani, *Nonlinear Fluid Dynamics from Gravity*, *JHEP* **02** (2008) 045 [arXiv:0712.2456] [InSPIRE].

[26] S. Grozdanov and N. Kaplis, *Constructing higher-order hydrodynamics: The third order*, *Phys. Rev. D* **93** (2016) 066012 [arXiv:1507.02461] [InSPIRE].

[27] X. Du, S. Ochsenfeld and S. Schlichting, *Universality of energy-momentum response in kinetic theories*, *Phys. Lett. B* **845** (2023) 138161 [arXiv:2306.09094] [InSPIRE].

[28] S. Ochsenfeld and S. Schlichting, *Hydrodynamic and non-hydrodynamic excitations in kinetic theory — a numerical analysis in scalar field theory*, *JHEP* **09** (2023) 186 [arXiv:2308.04491] [InSPIRE].

[29] I. Amado, C. Hoyos-Badajoz, K. Landsteiner and S. Montero, *Hydrodynamics and beyond in the strongly coupled N = 4 plasma*, *JHEP* **07** (2008) 133 [arXiv:0805.2570] [InSPIRE].

[30] J.F. Fuini, C.F. Uhlemann and L.G. Yaffe, *Damping of hard excitations in strongly coupled $\mathcal{N} = 4$ plasma*, *JHEP* **12** (2016) 042 [arXiv:1610.03491] [InSPIRE].

[31] T. Scopigno, G. Ruocco and F. Sette, *Microscopic dynamics in liquid metals: The experimental point of view*, *Rev. Mod. Phys.* **77** (2005) 881 [cond-mat/0503677] [InSPIRE].

[32] K. Trachenko and V.V. Brazhkin, *Collective modes and thermodynamics of the liquid state*, *Rept. Prog. Phys.* **79** (2015) 016502.

[33] S. Grozdanov, P.K. Kovtun, A.O. Starinets and P. Tadić, *Convergence of the Gradient Expansion in Hydrodynamics*, *Phys. Rev. Lett.* **122** (2019) 251601 [arXiv:1904.01018] [InSPIRE].

[34] S. Grozdanov, P.K. Kovtun, A.O. Starinets and P. Tadić, *The complex life of hydrodynamic modes*, *JHEP* **11** (2019) 097 [arXiv:1904.12862] [InSPIRE].

[35] M.P. Heller et al., *Convergence of hydrodynamic modes: insights from kinetic theory and holography*, *SciPost Phys.* **10** (2021) 123 [arXiv:2012.15393] [InSPIRE].

[36] M.P. Heller et al., *Relativistic Hydrodynamics: A Singulant Perspective*, *Phys. Rev. X* **12** (2022) 041010 [arXiv:2112.12794] [InSPIRE].

[37] M.P. Heller, R.A. Janik, M. Spaliński and P. Witaszczyk, *Coupling hydrodynamics to nonequilibrium degrees of freedom in strongly interacting quark-gluon plasma*, *Phys. Rev. Lett.* **113** (2014) 261601 [arXiv:1409.5087] [InSPIRE].

[38] L. Gavassino, M.M. Disconzi and J. Noronha, *Universality Classes of Relativistic Fluid Dynamics I: Foundations*, arXiv:2302.03478 [InSPIRE].

[39] L. Gavassino, M.M. Disconzi and J. Noronha, *Universality Classes of Relativistic Fluid Dynamics II: Applications*, arXiv:2302.05332 [InSPIRE].

[40] M. Stephanov and Y. Yin, *Hydrodynamics with parametric slowing down and fluctuations near the critical point*, *Phys. Rev. D* **98** (2018) 036006 [arXiv:1712.10305] [InSPIRE].

[41] A. Kurkela et al., *Effective kinetic description of event-by-event pre-equilibrium dynamics in high-energy heavy-ion collisions*, *Phys. Rev. C* **99** (2019) 034910 [arXiv:1805.00961] [InSPIRE].

[42] A. Kurkela et al., *Matching the Nonequilibrium Initial Stage of Heavy Ion Collisions to Hydrodynamics with QCD Kinetic Theory*, *Phys. Rev. Lett.* **122** (2019) 122302 [arXiv:1805.01604] [InSPIRE].

[43] X. Du and S. Schlichting, *Equilibration of the Quark-Gluon Plasma at Finite Net-Baryon Density in QCD Kinetic Theory*, *Phys. Rev. Lett.* **127** (2021) 122301 [arXiv:2012.09068] [InSPIRE].

[44] S. Kamata et al., *Hydrodynamization and nonequilibrium Green's functions in kinetic theory*, *Phys. Rev. D* **102** (2020) 056003 [arXiv:2004.06751] [InSPIRE].

[45] J. Brewer, L. Yan and Y. Yin, *Adiabatic hydrodynamization in rapidly-expanding quark-gluon plasma*, *Phys. Lett. B* **816** (2021) 136189 [arXiv:1910.00021] [InSPIRE].

[46] J. Brewer, W. Ke, L. Yan and Y. Yin, *Far-from-equilibrium slow modes and momentum anisotropy in expanding plasma*, arXiv:2212.00820 [InSPIRE].

[47] J. Brewer, B. Scheihing-Hitschfeld and Y. Yin, *Scaling and adiabaticity in a rapidly expanding gluon plasma*, *JHEP* **05** (2022) 145 [arXiv:2203.02427] [InSPIRE].

[48] S. Jaiswal et al., *Exact solutions and attractors of higher-order viscous fluid dynamics for Bjorken flow*, *Phys. Rev. C* **100** (2019) 034901 [arXiv:1907.07965] [InSPIRE].

[49] G.S. Denicol, H. Niemi, E. Molnar and D.H. Rischke, *Derivation of transient relativistic fluid dynamics from the Boltzmann equation*, *Phys. Rev. D* **85** (2012) 114047 [*Erratum ibid.* **91** (2015) 039902] [arXiv:1202.4551] [InSPIRE].

[50] Y. Akamatsu, A. Mazeliauskas and D. Teaney, *A kinetic regime of hydrodynamic fluctuations and long time tails for a Bjorken expansion*, *Phys. Rev. C* **95** (2017) 014909 [arXiv:1606.07742] [InSPIRE].

[51] H.B. Meyer, *Transport Properties of the Quark-Gluon Plasma: A Lattice QCD Perspective*, *Eur. Phys. J. A* **47** (2011) 86 [arXiv:1104.3708] [InSPIRE].

[52] H.B. Meyer, *Energy-momentum tensor correlators and spectral functions*, *JHEP* **08** (2008) 031 [arXiv:0806.3914] [InSPIRE].

[53] S. Borsányi et al., *High statistics lattice study of stress tensor correlators in pure* SU(3) *gauge theory*, *Phys. Rev. D* **98** (2018) 014512 [arXiv:1802.07718] [InSPIRE].

[54] J. Ghiglieri, G.D. Moore and D. Teaney, *Second-order Hydrodynamics in Next-to-Leading-Order QCD*, *Phys. Rev. Lett.* **121** (2018) 052302 [arXiv:1805.02663] [InSPIRE].